

Sources and characteristics of terrestrial carbon in Holocene-scale sediments of the East Siberian Sea

Kirsi Keskitalo¹, Tommaso Tesi^{1,3,4}, Lisa Bröder^{1,3}, August Andersson^{1,3}, Christof Pearce^{2,3}, Martin Sköld⁵, Igor P. Semiletov^{6,7,8}, Oleg V. Dudarev^{7,8} and Örjan Gustafsson^{1,3,*}

¹Department of Environmental Science and Analytical Chemistry, Stockholm University, Stockholm, SE 10691, Sweden

²Department of Geological Sciences, Stockholm University, Stockholm, SE 10691, Sweden

³Bolin Centre for Climate Research, Stockholm University, Stockholm, SE 10691, Sweden

⁴CNR-National Research Council of Italy, ISMAR-Marine Science Institute, Bologna, IT 40129, Italy

⁵Department of Mathematics, Stockholm University, Stockholm, SE 10691, Sweden

⁶International Arctic Research Center, University Alaska Fairbanks, Fairbanks, AK 99775, USA

⁷Pacific Oceanological Institute, Russian Academy of Sciences, Vladivostok, RU 690041, Russia

⁸Tomsk National Research Polytechnical University, Tomsk, RU 634050, Russia

*Correspondence to: Örjan Gustafsson (orjan.gustafsson@aces.su.se)

Abstract. Thawing of permafrost carbon (PF-C) due to climate warming can remobilise considerable amounts of terrestrial carbon from its long term storage to the marine environment. PF-C can be then buried in sediments or remineralised to CO₂ with implications for the carbon-climate feedback. Studying historical sediment records during past natural climate changes can help to understand the response of permafrost to current climate warming. In this study, two sediment cores collected from the East Siberian Sea were used to study terrestrial organic carbon sources, composition and degradation during the past ~9,500 cal yrs BP. ~~The~~ CuO-derived lignin and cutin products- (*i.e. compounds solely biosynthesised in terrestrial plants*) combined with δ¹³C suggest that there was a higher input of terrestrial organic carbon to the East Siberian Sea between ~9,500 and 8,200 cal yrs BP than in all later periods. This high input was likely caused by marine transgression and permafrost destabilisation in the early Holocene climatic optimum. Based on source apportionment modelling using dual-carbon isotope (Δ¹⁴C, δ¹³C) data, coastal erosion releasing old Pleistocene permafrost carbon was identified as a significant source of organic matter translocated to the East Siberian Sea during the Holocene.

31 1 Introduction

32 The amount of organic carbon (OC) stored in the northern circumpolar permafrost (PF) amounts to ~1300 Pg
33 OC of which ~800 Pg OC is perennially frozen (the remaining 500 Pg is non-permafrost, seasonally thawing
34 active-layer permafrost or taliks) (Hugelius et al. 2014). Northern [hemisphere](#) circumpolar soils thereby hold
35 roughly half of the global soil OC pool (Tamocai et al., 2009). Modelled future climate scenarios predict
36 continued amplified warming in the Arctic for the coming 100 years (IPCC, 2013). This will further destabilise
37 permafrost, leading to increased delivery of terrestrial OC to the Arctic Ocean. The potential decomposition of
38 this relict permafrost carbon (PF-C) and its subsequent release to the atmosphere as CO₂ or CH₄ constitutes a
39 positive feedback to global warming (IPCC, 2013; Koven et al., 2011; Schuur et al., 2015; [Shakhova et al.,
40 2013, 2015, 2009](#); Vonk and Gustafsson, 2013). Considering the size of the Arctic PF-C pool it is important to
41 better understand the dynamics and extent of its vulnerability to remobilisation in response to climate warming.

Field Code Changed

42 Many recent studies have focused on current carbon cycling in the Arctic land-ocean continuum
43 ([Anderson et al., 2009, 2011](#); [Bröder et al., 2016a](#); [Goñi et al., 2013](#); [Goñi et al., 2000](#); [Karlsson et al., 2015](#);
44 [Semiletov et al., 2016, 2011, 2012](#); [Shakhova et al., 2010](#); [Tesi et al., 2014, 2016b](#); [Vonk et al., 2010](#);
45 [Winterfeld et al., 2015b](#)) with possible linkages to climate change. Constraining how this system responded to
46 earlier climate warming may help us to better predict the future response of PF-C and its climate couplings. The
47 last glacial-interglacial transition constituted a major climate rearrangement on Earth. The increase in mean
48 temperature coupled with sea level rise is thought to have profoundly destabilised PF-C and further released
49 CO₂ to the atmosphere (Ciais et al. 2013; Crichton et al. 2016; [Köhler et al. 2014](#); Tesi et al. 2016a). Several
50 studies have suggested that there was a warming-coupled translocation of terrestrial carbon during the climate
51 warming that ended the latest glacial period (e.g., Bauch et al. 2001; Ciais et al. 2013; Mueller-Lupp et al. 2000;
52 Tesi et al. 2016a) similar to what is predicted to happen as a consequence of the anthropogenic climate change
53 (Barnhart et al. 2014; Vonk and Gustafsson 2013).

Field Code Changed

54 Many of the previous Holocene timescale studies in the East Siberian Arctic Shelf (ESAS) have
55 focused on the Laptev Sea (e.g., Bauch et al., 2001b; Mueller-Lupp et al., 2000; Tesi et al., 2016a). This study
56 focuses on the East Siberian Sea (ESS) which has not yet been extensively studied [in this aspect especially for
57 the historical reconstruction of PF-C dynamics.](#) The ESS receives terrestrial OC by coastal erosion, fluvial
58 inflow and possibly sea bed erosion (Karlsson et al., 2016; Semiletov et al., 2005; Stein and Macdonald, 2004;
59 Tesi et al., 2014, 2016b; Vonk et al., 2010). The coast of the ESS is dominated by carbon-rich Ice Complex
60 Deposits (ICD) consisting of old Pleistocene material (Schirrneister et al. 2011; Semiletov 1999a, 1999b; Vonk
61 et al. 2012). These large ICD bluffs are vulnerable to coastal erosion (Semiletov et al., 2013; Stein and
62 Macdonald 2004; Schirrneister et al. 2011; Vonk et al. 2012). Coastal erosion can be further intensified with
63 warming enhanced processes like loss of sea ice cover, increasing frequency of storms, degradation of ice-
64 bonded coasts and sea level rise (Barnhart et al., 2014; Jones et al., 2009; Stein and Macdonald, 2004). The
65 largest rivers directly emptying into the ESS are Indigirka and Kolyma with suspended matter discharge of 11.1
66 x 10¹² g yr⁻¹ and 123±19 x 10⁹ g yr⁻¹ (Gordeev, 2006; McClelland et al., 2016, respectively), with an input also
67 from the Lena River. The Lena River drains into the Laptev Sea but its exported terrestrial OC is also
68 transferred to the ESS via the Siberian Coastal Current (e.g., Alling et al., 2012; Sánchez-García et al., 2011).
69 However, studies by Vonk et al. (2010, 2012) suggest that the contribution of ICD-PF erosion to the ESS
70 sediment OC dominates over river discharge (ranging from 36 to 76 % in comparison to 5–35 %, respectively).
71 [Similar observation have been made in the Laptev Sea by Semiletov et al., \(2005, 2011, 2012\) and Vonk et al.,](#)

Field Code Changed

Field Code Changed

72 | ~~(2012, 2014) concluding that the effect of the Lena River input is overall smaller than that from the coastal~~
73 | ~~erosion.~~

74 | In this study we investigate land-to-ocean transfer and fate of PF-C ~~from during the latest state of the~~
75 | ~~last~~-post-glacial eustatic sea level rise until the present day. Our main objectives are to determine the sources
76 | and remobilisation fluxes of terrestrial OC as well as the composition and degradation status of the OC that was
77 | buried in ESS sediments during the Holocene. We characterise the OC composition by quantifying lignin
78 | phenols, cutin acids and other compounds yielded upon CuO oxidation to constrain the sources and degradation
79 | status of PF-C as well as the contribution of marine OC. Furthermore, we use a mixing model based on the
80 | isotopic composition ($\Delta^{14}\text{C}$, $\delta^{13}\text{C}$) of the deposited OC to quantify the contribution of three different sources:
81 | topsoil-PF from active-layer deepening, ICD-PF and marine plankton. Additionally, we study how OC
82 | deposition fluxes have changed over time in response to the sea level rise and Holocene warming.

83 2 Materials and methods

84 2.1 Background and study area

85 The ~~East Siberian Sea (ESS)~~ is located off the northeast Siberian coast between the Laptev Sea and the Chukchi
86 Sea (Fig. 1). The ESS is one of the largest shelf seas (987,000 km²) in the Arctic Ocean as well as one of the
87 shallowest (mean depth 52 m) (Jakobsson, 2002).

88 Thermokarst landscapes (i.e. thawing ice-rich permafrost) cover ~20 % (3.6 x 10⁶ km²) of the northern
89 circumpolar permafrost region (Olefeldt et al., 2016). Ice Complex Deposit and thermokarst landscapes cover
90 2,400 km of the ESS coastline (Grigoriev and Rachold 2003). The modern average rate of coastal retreat in the
91 ESS and the adjacent Laptev Sea is 1–10 m yr⁻¹ (Grigoriev 2010), though locally, even higher retreat rates (up to
92 24 and 30 m yr⁻¹) have been reported in the most actively eroding parts (Kanevskiy et al., 2016; Romanovskii et
93 al., 2004). The coastal erosion rates have increased in the Arctic in recent decades (Barnhart et al., 2014;
94 Günther et al., 2015; Jones et al., 2009). According to recent studies (e.g., Bröder et al., 2016a; Semiletov et al.,
95 2013; Tesi et al. 2016b; Vonk et al. 2012) a large fraction of the remobilised PF-C is degraded during cross-
96 shelf transport and released back to the contemporary carbon cycle. To better predict the consequences of the
97 permafrost thaw, it is important to understand both the amount of remobilised organic carbon as well as its fate.

98 The shelf of the ~~East Siberian Sea~~ESS -contains terrestrial permafrost formed during the sea level low
99 of last glacial maximum (Jakobsson et al. 2014). During the Pleistocene-Holocene transition the ESAS was
100 flooded when the sea level rose rapidly (Lambeck et al., 2014; Mueller-Lupp et al., 2000). This global marine
101 transgression started ~20,000 cal yrs BP (Lambeck et al., 2014) and flooded the ESAS between ~11,000 to
102 ~7,000 cal yrs BP (Bauch et al. 2001a; Mueller-Lupp et al. 2000). The rate of the sea level rise was in order of 1
103 cm yr⁻¹ or more (Cronin et al., 2017; Stanford et al., 2010) in the early Holocene. The sampling site of the
104 sediment core investigated in this study was flooded around 11,000 cal yrs BP (Lambeck et al., 2014). The early
105 Holocene temperatures in the Arctic regions were on average 1.6±0.8°C higher than today (Kaufman et al.,
106 2004) and the sea ice was at a low (Fisher et al., 2006).

107 Post-glacial sea level rise with warming and wetting of the climate caused a major relocation of
108 permafrost carbon from land to the Arctic Ocean (Bauch et al. 2001; Tesi et al. 2016a). ~~Today the period with~~
109 ~~less sea ice in the ESS is on average 3 months per year which is one of the reasons why the area remains fairly~~
110 ~~unstudied (Stein and Macdonald, 2004; Vetrov and Romankevich, 2004).~~ Today the period when the ESS is
111 only partially covered with sea ice is on average 3 months per year which is one of the reasons why the area
112 remains fairly unstudied (Stein and Macdonald, 2004; Vetrov and Romankevich, 2004).

114 2.2 Sampling

115 A gravity core (called GC58) was collected in the ~~East Siberian Sea-ESS~~ -at 54 m water depth as a part of the
116 international SWERUS-C3 research expedition on ~~the~~ AB/B -Oden in ~~July~~ August 2014. The coring site (Leg 1,
117 station 58, 74.4387° N, 166.0467° E) is located ~500 km from the modern shoreline (Fig. 1). An additional
118 sediment core was collected at the same site (MUC58) using a sediment multicorer (Oktopus GmbH, Germany),
119 which is specifically designed to preserve the sediment-water interface. The total length of GC58 was 78 cm
120 while MUC58 was 32 cm long. The GC58 core was split in half during the expedition and kept refrigerated (+4°
121 C). In the laboratory at Stockholm University, one half was subsampled at 1 cm intervals and kept frozen at -18°
122 C. The multicore was sliced during the expedition at 1 cm intervals and then immediately frozen (-18° C). Prior
123 to analyses, the samples were freeze-dried at the Department of Environmental Science and Analytical
124 Chemistry, Stockholm University, Sweden.

Field Code Changed

125

126 **2.3 ²¹⁰Pb dating**

127 Radiogenic ²¹⁰Pb was analysed with a gamma-ray spectrometer (GRS) at the Department of Geology of the
128 Swedish Museum of Natural History in Stockholm, Sweden. The GRS determines the decay energy of
129 radioisotopes in counts per second by measuring gamma emission of the sample at a known energy level.

130 Prior to the GRS analysis, a subsample of approximately 10 g was homogenised and placed in a plastic
131 container for at least three weeks to reach secular equilibrium between the radioisotopes of lead and radium
132 (²¹⁰Pb and ²²⁶Ra, respectively). The samples were analysed for ²¹⁰Pb (46.51 keV), ²²⁶Ra (186.05 keV) and ¹³⁷Cs
133 (661.66 keV) on an EG&G ORTEC® co-axial low energy photon spectrometer containing a High-Purity
134 Germanium detector. The counting period for each sample lasted from 1–3 days depending on the amount of
135 ²¹⁰Pb in the sample. An externally calibrated U-series standard (pitchblende, Stackebo, Sweden) was used to
136 determine the relative efficiency of the gamma detector system. For each sample a minimum of 350 counts was
137 acquired. A blank (empty container) sample was measured to correct for the background activity. The original
138 method is described in detail by Elmquist et al., (2007).

139 Two different models were used for the ²¹⁰Pb dating: CRS (constant rate of supply) model which
140 assumes a constant rate of supply of excess ²¹⁰Pb fallout, and CIC (constant initial concentration) model which
141 assumes constant initial concentration of excess ²¹⁰Pb (Appleby and Oldfield, 1977).

142

143 **2.4 Bayesian modelling of ¹⁴C ages for the chronology**

144 For the age-depth model construction, molluscs retrieved ([handpicked](#)) from GC58 were analysed for their
145 radiocarbon (¹⁴C) content at the US-NSF National Ocean Sciences Accelerator Mass Spectrometry (NOSAMS)
146 Facility at the Woods Hole Oceanographic Institution (WHOI), MA, USA. [Prior to the analysis the mollusc](#)
147 [shells were rinsed with MilliQ water and sonicated.](#) The analysis followed ~~their~~ standard procedures of
148 [NOSAMS](#) (Pearson et al., 1998) (Table 1).

149 To account for natural differences in the amount of ¹⁴C in the atmosphere as well as differences
150 between the marine environment and the atmosphere (e.g., Stuiver and Braziunas 1993), all ¹⁴C data were
151 calibrated with the Marine13 calibration curve ([Reimer et al., 2013](#)). The offset in the local reservoir age was
152 taken into account by using a ΔR of 50 ± 100 years. Since there are no ΔR values for the ESS in the literature,
153 this ΔR value was taken from a study in the Laptev Sea (Bauch et al. 2001a). The radiocarbon dates are reported
154 in [conventional radiocarbon ages-calendar years before present](#) (cal yrs BP) (Stuiver and Polach 1977).

155 The age model of the core was built with the OxCal v4.2 program based on the radiocarbon dated
156 molluscs and a depositional model (P_sequence, $k = 0.5$) (Bronk Ramsey 2008; Bronk Ramsey and Lee 2013).
157 Also, the base of the adjacent multicore dated with ²¹⁰Pb was used in the model. The ²¹⁰Pb date used was an
158 average age (50 yrs BP) from the two ²¹⁰Pb dating models (CRS, CIC) for the bottom layer (12.5 cm) of the
159 multicore (Supplementary Table S3). The age model of GC58 was constructed with a Bayesian statistics
160 approach using the reservoir age (ΔR) and the depth as a prior model and measured radiocarbon dates as
161 likelihoods. The posterior probability densities were acquired with a Markov Chain Monte Carlo procedure
162 which calculates possible distributions in order to date each sediment layer using the given prior model and
163 likelihoods (Bronk Ramsey 2008).

164 Sampling with a heavy gravity corer often disturbs the sediment-water interface and thereby causes
165 losses of the surface sediments. The organic carbon (OC) content of GC58 was therefore compared to the OC

166 content of the adjacent MUC58 to identify for the possible loss. According to the comparison, the top 3 cm were
167 likely lost in GC58 (Supplementary Fig. S1), and thus corrected for.

168 2.5 Alkaline CuO oxidation

169 Microwave assisted alkaline CuO oxidation was carried out using the method by Goñi and Montgomery (2000).
170 Each homogenised subsample of around 300 mg was mixed with 300 mg of cupric oxide (CuO) and 50 mg of
171 ammonium iron (II) sulphate hexahydrate ((NH₄)₂Fe(SO₄)₂·6H₂O). After thorough mixing, nitrogen-purged 2M
172 NaOH was added to each sample. Alkaline oxidation was performed with an UltraWAVE Milestone 215
173 microwave digestion system at 150°C for 90 min.

174 A known amount of internal recovery standards (ethyl-vanillin, cinnamic acid) was added to the CuO
175 reaction products and then acidified to pH 1 with concentrated HCl (35 %). The CuO reaction products were
176 repeatedly extracted using ethyl acetate (EtOAc). Anhydrous sodium sulphate (NaSO₄) was added to remove the
177 remaining water. The extracts were dried in a CentriVap (Christ RVC 2-25) at 60° C, re-dissolved in pyridine
178 and stored in a freezer (-18° C) until further analysis.

179 Finally, the samples were analysed with a gas chromatograph mass spectrometer (GC-MS, Agilent
180 7820A) using a DB5-MS capillary column (60 m x 250 µm, 0.25 µm stationary phase thickness, Agilent J&W)
181 at an initial temperature of 60° C, followed by a ramp of 5° C/min until reaching 300° C. Prior to the GC-MS
182 analysis, the extracts were derivatised with *bis-trimethylsilyl trimethylsilyl* trifluoroacetamide (BSTFA) + 1 %
183 trimethylchlorosilane (TMCS) to silylate exchangeable hydrogens. The quantification of the samples was based
184 on the comparison of the key ions to commercially available standards. Concentrations of CuO oxidation
185 products were normalised to the organic carbon content of the sample and are reported as mg g⁻¹ OC.
186

187 2.6 Bulk organic carbon and stable carbon isotope analyses

188 For the total organic carbon content (TOC), the total nitrogen content (TN) and the stable carbon isotope
189 analysis (δ¹³C) of TOC, subsamples of 10–15 mg were homogenised and placed in silver capsules, acidified
190 with 1.5M HCl to remove carbonates and then dried at 60° C. The TOC, TN and δ¹³C-TOC were quantified with
191 an elemental analyser Carlo Erba NC2500 connected via a split interface to a Finnigan MAT Delta V mass
192 spectrometer at the Stable Isotope Laboratory of the Department of Geological Sciences at Stockholm
193 University.

194 For radiocarbon (¹⁴C) analysis of the bulk organic carbon, subsamples of sediment were acidified with
195 1.5M HCl and sent to NOSAMS. To account for the time between the deposition and the measurement, the ¹⁴C
196 dates were calibrated with the Eq. (1) using the age data derived from the age model. The bulk radiocarbon data
197 are reported as Δ¹⁴C (Stuiver and Polach 1977).

$$198 \Delta^{14}\text{C} = (\text{Fm} \times e^{\lambda(1950-Y_c)} - 1) \times 1000 \quad (1)$$

199 where Fm is the Fraction Modern, λ is 1/mean life of radiocarbon= 1/8267 and Yc is the year of collection
200 derived from the age model (Stuiver and Polach, 1977).

204 2.7 Source apportionment

205 The carbon isotope fingerprint of OC (Δ¹⁴C, δ¹³C) can be used to quantitatively diagnose the relative
206 contribution of topsoil-PF, ICD-PF and marine OC assuming isotopic mass balance (e.g., Vonk et al., 2012). In
207 other words, the carbon isotopic signatures may help to understand whether the OC comes from coastal erosion
208 as a result of the post-glacial warming and sea level rise, active-layer deepening of permafrost carbon in the

209 watershed (as a response to the post-glacial warming) or sedimentation of marine phytoplankton. These different
210 sources have a natural variability in their isotopic composition (end-members). This variability needs to be taken
211 into account to correctly estimate the relative source contributions and the associated uncertainties (e.g.,
212 Andersson, 2011). In previous studies a Bayesian Markov Chain Monte Carlo (MCMC) driven approach has
213 been used to ~~effectively~~ estimate the relative source contributions for individual data points (Andersson et al.,
214 2015; Tesi et al., 2016a). Here, we expand this approach to include the time-dependence of the down-core
215 isotopic signatures, taking an advantage of the relatively small variability of the 78 $\delta^{13}\text{C}$ data points, whilst also
216 using the 10 $\Delta^{14}\text{C}$ points. The time-dependence of different proportions was taken into account by following the
217 approach of Parnell et al. (2012, 2013). The method is described in detail in the Supplementary Methods.

218 The end-member values for the three source classes were taken from the literature (~~Bröder et al.,~~
219 ~~2016b; Tesi et al., 2016a~~) (ICD-PF and topsoil-PF values compiled in Vonk et al., 2012; marine OC from Smith
220 et al., 2002) topsoil-PF ($\Delta^{14}\text{C} = 232 \pm 147 \text{‰}$, $\delta^{13}\text{C} = 26.95 \pm 1.17 \text{‰}$; ($\Delta^{14}\text{C} = -126 \pm 54 \text{‰}$, $\delta^{13}\text{C} = -28.2 \pm 1.96 \text{‰}$;
221 mean \pm standard deviation), representing thaw of the active-layer of permafrost; marine OC ($\Delta^{14}\text{C} = -50 \pm 12 \text{‰}$,
222 $\delta^{13}\text{C} = 20.97 \pm 2.56 \text{‰}$) ($\Delta^{14}\text{C} = -60 \pm 60 \text{‰}$, $\delta^{13}\text{C} = -21 \pm 1 \text{‰}$), resulting from primary production of phytoplankton;
223 and ICD-PF ($\Delta^{14}\text{C} = 940 \pm 31 \text{‰}$, $\delta^{13}\text{C} = 26.3 \pm 0.63 \text{‰}$) ($\Delta^{14}\text{C} = -940 \pm 84 \text{‰}$, $\delta^{13}\text{C} = -26.3 \pm 0.63 \text{‰}$), resembling the
224 old Pleistocene material from coastal erosion. The end-member value for ICD-PF was corrected with Eq. (1) to
225 account for the age of the deposition.

226

227 2.8 Grain size analysis

228 Prior to the grain size analysis subsamples of sieved (500 μm) sediments from GC58 were homogenised. The
229 grain size analysis was done with a Malvern Mastersizer 3000 laser diffraction particle size analyser, which can
230 measure particles between 10 nm and 3.5 mm. Sodium ~~hexametaphosphate~~ ~~hexametaphosphate~~ (10 %) was used
231 to disaggregate the particles suspended in deionised water. To further aid the disaggregation, all samples were
232 exposed to ultrasound for 60 s and allowed to disperse in continuous flow for 3 min in total (including 60 s of
233 ultrasonication) prior to the measurements. To control the concentration of the sample in the flow during the
234 measurements, the obscurity was kept between 5–15 %. High sample obscurity (i.e. high concentration) would
235 cause multiple light scatterings, thus distorting the results. Each sample was analysed in five replicates. The
236 measurements were carried out at the Department of Geological Sciences at Stockholm University, Sweden.

237 3 Results and Discussion

238 3.1 Age chronology of the core

239 The deepest part of the sediment core GC58 dates back ~9,500 cal yrs BP i.e. to the early Holocene. The age-
240 depth model shows an evident hiatus in the middle of the core between 39.5 cm and 40.5 cm resulting in an age
241 gap of ~6,500 years (~8,200–1,700 cal yrs BP) (Fig. 2). In addition, there is a shorter gap in the chronology
242 between ~9,300 and ~8,500 cal yrs BP. In studies from the adjacent Laptev Sea such age discrepancies have not
243 been observed (Bauch et al. 2001a; Bauch et al. 2001b; Tesi et al. 2016a). It therefore seems likely that there has
244 been a local event causing the removal of sediment layers. There might not have been accumulation during
245 those periods, or the age gap could be a condensed unit of sediment. ~~Although any An~~ actual sediment transport
246 processes giving rise to such a putative total halt in the sedimentation rate is rather elusive and unlikely. Since
247 the whole ~~East Siberian Arctic Shelf~~ (ESAS) is a very shallow shelf where sea ice is formed (Conlan et al.,
248 1998; Jakobsson, 2002), ~~a likely another~~ explanation for an age gap is ice scouring as observed in the Laptev
249 Sea (Ananyev et al., 2016), ~~e, specially at ~8,500 cal yrs BP when the sea level was around 18 m lower~~
250 ~~(Lambeck et al., 2014) than today and the water depth at the coring site was around 32 m. At the time of the~~
251 ~~second age gap (~1,700 cal yrs BP) the water depth at the coring site was approximately 52 m.~~ An ice scouring
252 event could have formed a gouge at the sea bottom that later was re-filled with sediment (Barnes et al. 1984).

Field Code Changed

253 The accumulation rates of GC58 obtained from the ^{14}C measurements vary between 0.2 and 1.4 mm yr $^{-1}$
254 (17.0–138.9 cm kyr $^{-1}$) and mass accumulation rates (MAR) spanned 0.02–0.1 g cm $^{-2}$ yr $^{-1}$. Bauch et al. (2001a)
255 have reported similar sedimentation rates (0.1–2.6 mm yr $^{-1}$) from the outer shelf of the Laptev Sea around the
256 same time period. The linear sedimentation rate for the adjacent sediment core MUC58 derived from ^{210}Pb
257 dating is 1.3 mm yr $^{-1}$ and an average MAR 0.03 g cm $^{-2}$ yr $^{-1}$. Similar accumulation rates with ^{210}Pb dated sediment
258 cores have been reported in other studies from the ~~East Siberian Sea~~ ESS: 1.1–1.6 mm yr $^{-1}$ (Vonk et al. 2012)
259 and 1.4–1.5 mm yr $^{-1}$ (Bröder et al., 2016b). The slight difference in accumulation rates using ^{210}Pb chronology
260 compared to ^{14}C may be due to active biological mixing giving higher accumulation rates for the shorter time
261 scale of more surficial sediments (Baskaran et al. 2016; Boudreau 1994).

262

263 3.2 Sediment grain size, stable carbon isotopes and biomarker composition of organic matter

264 Grain size can be used to describe the depositional environment. The sediment core GC58 consists mostly of
265 clay and silt, with a fraction of sand (Supplementary Fig. S2). The higher sand content that is observed at ~8,500
266 cal yrs BP may reflect a higher-energy depositional regime likely due to proceeding marine transgression and
267 energetic coastal dynamics. Bauch et al. (2001a) have reported a shift from sandy silt to clayey silt around 7,400
268 cal yrs BP from a sediment core collected in the eastern Laptev Sea. They attribute this change to the end of the
269 sea level rise and the establishing of more stable conditions. The GC58 sediment core has a hiatus at that time
270 period, but has a similar clayey silt composition at the top part of the core (~1,700 cal yrs BP until today). This
271 may indicate comparably similar stable conditions in the ~~East Siberian Sea~~ ESS in the last 1,700 cal yrs BP.

272 The total organic carbon (TOC) concentrations in GC58 vary from 0.5 to 1.1% (Supplementary Table
273 S1) with the highest TOC content in the surface sediments. These data agree with average TOC contents
274 reported for the ~~ESS East Siberian Sea~~ (Semiletov et al., 2005; Stein and Macdonald, 2004; Vetrov and
275 Romankevich, 2004; Vonk et al., 2012). The OC fluxes for GC58 calculated with the ^{14}C age-model (covering
276 ~9,500 cal yrs BP) range between 1.2 and 10.9 g m $^{-2}$ yr $^{-1}$ (Fig. 3a). The OC fluxes for MUC58 calculated with
277 the ^{210}Pb chronology (covering the most recent ~100 yrs) are similar and vary from 0.4 to 6.1 g m $^{-2}$ yr $^{-1}$
278 (Supplementary Table S2). The OC fluxes show an increasing trend from the bottom of the core toward the top

279 | in both cores. A similar trend has been reported by (Bröder et al., 2016b) from the ~~ESS East Siberian Sea~~ using
280 | two ²¹⁰Pb-dated sediment cores. For GC58, the high OC flux at the very top of the core is likely related to the
281 | merging of the two dating systems (¹⁴C and ²¹⁰Pb), which causes a higher sediment accumulation rate at the top
282 | of the core and thus higher fluxes.

283 | Lignin phenols and cutin acids are useful proxies for tracing carbon of terrestrial origin because both
284 | compounds are solely biosynthesised in terrestrial plants. Lignin is an essential component in cell walls of
285 | vascular plants (Higuchi, 1971), while cutin is a lipid polyester, which forms a protective wax layer on
286 | epidermal cells of leaves and needles with other lipids (e.g., Kunst and Samuels 2003). ~~These compounds have~~
287 | ~~been widely used in recent studies of terrestrial OC in the Arctic~~ These compounds have been demonstrated to be
288 | useful in studying terrestrial OC in the Arctic (e.g., Amon et al., 2012; Bröder et al., 2016b; Goñi et al., 2013;
289 | Tesi et al., 2014). Both lignin and cutin fluxes show a similar trend with the highest fluxes at the bottom of the
290 | core (~9,500 cal yrs BP) indicating a high proportion of terrestrial organic matter (Fig. 3b). The large variability
291 | in the fluxes between ~9,500 and ~8,200 cal yrs BP compared to the latest ~1,700 cal yrs BP suggests that the
292 | system was more dynamic at that time. The rapid decrease in both lignin and cutin fluxes proposes a change
293 | from terrestrially dominated to marine dominated input at ~8,400 cal yrs BP in this part of the ~~ESS East~~
294 | ~~Siberian Sea~~. Bauch et al. (2001b) suggested a similar regime shift from terrestrial to marine in the Laptev Sea
295 | between ~8,900 and ~8,400 cal yrs BP based on the occurrence of bivalves and benthic foraminiferal species.
296 | The same process affecting OC fluxes is likely causing also higher lignin and cutin fluxes at the top of GC58.
297 | The overall decrease in lignin and cutin fluxes as well as concentrations (Supplementary Table S3) in time is
298 | likely due to increasing hydrodynamic sorting and degradation during transport as transport times from the coast
299 | became longer because of the marine transgression (Fig. 3a). Bröder et al., (2016a) have observed a similar
300 | strong decrease in the amount of terrestrial organic carbon depositions with increasing distance from the coast in
301 | the Laptev Sea. A recent study by Tesi et al. (2016b) shows that the largest particles, rich in lignin (i.e. plant
302 | debris), tend to be preferentially buried close to the shore and with cross-shelf transport of lignin occurring
303 | overwhelmingly bound to fine particles (with low settling velocities) (i.e. of the total lignin deposited to the
304 | marine environment only a fraction, ~4–5 %, travels across the shelf).

305 | Other useful indicators of the marine input in organic matter are CuO oxidation derived low-molecular
306 | weight fatty acids (LMW-FA). They are mainly found in phytoplankton but also in other organisms such as
307 | bacteria and algae (Goñi and Hedges, 1995). Especially C16FA:1 together with C14FA and C16FA serve as
308 | proxies for marine OC as they are highly abundant in marine sediments and very low in concentrations in ICD-
309 | PF and topsoil-PF (Goñi and Hedges, 1995; Tesi et al., 2014). The highest fluxes of LMW-FA are observed for
310 | the very top of the core (Fig. 3c), indicating a larger proportion of marine OC. The values decrease rapidly
311 | down-core as marine FA are readily degraded (e.g., Bröder et al., 2016b; Canuel and Martens, 1996). This trend
312 | may also be influenced by the change in input from terrestrial to marine dominated sources.

313 | The stable isotopic composition of bulk OC ($\delta^{13}\text{C}$) may be used to distinguish between marine and
314 | terrestrial organic matter (Fry and Sherr, 1984). The $\delta^{13}\text{C}$ values for C3-photosynthesised terrestrial carbon are
315 | between -23 to -30 ‰, whereas marine carbon has a less depleted $\delta^{13}\text{C}$ signature between -18 ‰ and 24 ‰ (e.g.,
316 | Fry and Sherr, 1984). However, these end-member values may differ depending on the region, especially in the
317 | Arctic where open water and sea ice phytoplankton exhibits different isotopic fingerprints (Kohlbach et al.,
318 | 2016). The $\delta^{13}\text{C}$ values for GC58 range from -23 to -25 ‰ (Fig. 3d) with the most depleted values (i.e. most
319 | terrestrial) between ~9,500 and ~8,200 cal yrs BP, and the least depleted values (i.e. most marine) from ~1,700

320 cal yrs BP until the modern time. Mueller-Lupp et al. (2000 and references within) have argued that $\delta^{13}\text{C}$ values
321 in sediments of the Arctic Ocean can have a terrestrial overprint in $\delta^{13}\text{C}$ composition caused by the rapid
322 degradation of planktonic organic matter i.e. the amount of marine organic matter of the total organic matter
323 pool in the Arctic is relatively low. Yet, the gradual change in $\delta^{13}\text{C}$ indicates that the contribution of marine
324 organic matter is greater at the top of the core where the $\delta^{13}\text{C}$ values are less depleted.

325 It is notable that the values for all the different parameters shown in Fig. 3 on both sides of the age gap
326 (between ~8,200 and ~1,700 cal yrs BP) are near-continuous in spite of the ~6,500 year hiatus (except for the
327 bulk $\Delta^{14}\text{C}$ OC values). ~~Either the values actually are similar in both sides of the hiatus or alternatively t~~This
328 could be explained by bioturbation, mixing the older part of the core with the newer deposits, thus resulting in
329 an apparent continuity in property values across the hiatus. The $\Delta^{14}\text{C}$ values suggest that there was more ^{14}C
330 depleted material deposited ~1,600 cal yrs BP ago, causing a drop in the $\Delta^{14}\text{C}$ values. Though more likely, as
331 the $\Delta^{14}\text{C}$ values are dependent on time, any uncertainty in the age model would have an effect on the $\Delta^{14}\text{C}$
332 values.

333

334 3.3 Degradation status of terrestrial organic matter

335 Lignin phenols provide insight into the degradation status of the deposited terrestrial organic matter. The acid-
336 to-aldehyde ratios of lignin phenols, syringic acid to syringaldehyde (Sd/SI) and vanillic acid to vanillin
337 (Vd/VI), have been used to study degradation of lignin (e.g., ~~Benner and Opsahl and Benner~~, 1995; Hedges et
338 al., 1988). ~~As acids are more abundant in relation to aldehydes in degraded lignin, higher ratios mean more~~
339 ~~degraded lignin (Goñi et al., 1993). Both Sd/SI and Vd/VI ratios show great variability throughout the core (Fig.~~
340 ~~4a), especially for the top part of the core. The variability at the core top may reflect the analytical uncertainty~~
341 ~~caused by very low lignin concentrations. In addition, However,~~ Goñi et al. (2000) and Tesi et al. (2014) have
342 argued that the acid to aldehyde ratios of lignin phenols might not serve as good degradation proxy for Arctic
343 Ocean sediments as the material entering the marine environment might have experienced degradation prior to
344 entering the marine system. This is supported by our data as both Sd/SI and Vd/VI ratios show great variability
345 throughout the core (Supplementary Fig. S3).

346 The ratio of 3,5-dihydrobenzoic acid to vanillyl phenols (3,5-Bd/V) is another proxy used to constrain the
347 degradation status of terrestrial organic matter in sediments (e.g., Hedges et al. 1988; Tesi et al. 2014; Tesi et al.
348 2016a). Specifically, this proxy is used to distinguish diagenetically-altered mineral soil OC from relatively
349 fresh vascular plant debris (Farella et al. 2001; Louchouart et al. 1999; Prah et al. 1994). The only source of
350 3,5-Bd in the marine environment is from brown algae which are not common in the study area (Goñi and
351 Hedges, 1995; Tesi et al., 2014). The low 3,5-Bd/V ratio at the bottom of the core (~9,500– 8,200 cal yrs BP)
352 implies that the organic matter that was deposited in that period was relatively undegraded ~~-(Supplementary Fig.~~
353 ~~S3) (Fig. 4b)~~. The extent of degradation gradually increases toward the top of the core. However, hydrodynamic
354 sorting may affect the degradation values as the largest particles of fresh vascular plant debris are likely buried
355 close to the coast (Tesi et al., 2016b). The input of organic matter was higher before ~8,200 cal yrs BP,
356 presumably due to coastal erosion caused by the marine transgression. When sediments are quickly buried they
357 can serve as a more effective sink for terrestrial organic matter (Hilton et al., 2015). As the material is less
358 degraded and the sedimentation rates are high in GC58 between ~9,500 and ~8,200 cal yrs BP, the input of
359 organic matter was likely high causing it to be quickly buried. Similar high input of terrestrial material has been
360 observed in the Laptev Sea ~11,000 cal yrs BP (Tesi et al. 2016a).

Field Code Changed

361 The location of the study site is currently ~500 km offshore so transport time and thereby the oxygen
362 exposure time of the organic matter in the benthic compartment is now longer than in the earlier phase of the
363 Holocene. The longer distance from the coast allows more time for organic matter to degrade before burial
364 (Bröder et al., 2016a). Hartnett et al. (1998) have also shown that the burial efficiency of organic carbon
365 decreases as a function of oxygen exposure time. The same trend can be seen in the fraction remaining lignin
366 ($f_{\text{lignin/terrOC}}$) i.e. the amount of lignin as a ratio of the observed and expected (assuming conservative mixing i.e.
367 no degradation) concentrations of lignin and terrestrial OC (terrOC) (see Supplementary Methods for details). In
368 GC58 the $f_{\text{lignin/terrOC}}$ decreases down-core likely as a result of the preceding marine transgression
369 (Supplementary Fig. S43). This trend suggests that with longer transport time the lignin degradation is more
370 extensive due to the protracted oxygen exposure time and hydrodynamic sorting (Keil et al., 2004; Tesi et al.,
371 2016a). We estimated this lateral transport time to be ~1.4 kyr longer at modern times than at the beginning of
372 the Holocene for the station GC58 (Supplementary Fig. S54). To model the lateral transport times, we used the
373 $f_{\text{lignin/terrOC}}$ with individual degradation rates for terrOC and lignin (Bröder et al. 2017, submitted) (see
374 Supplementary Methods).

375

376 3.4 Dual-isotope based source apportionment of OC

377 The source apportionment results show that most of the organic matter originates from coastal erosion since
378 ICD-PF material is the largest fraction (41–91 %) throughout the core (Fig. 5). Earlier studies demonstrated that
379 the decay of fresh marine organic matter is more rapid compared to degradation of terrestrial organic matter
380 (Karlsson et al., 2011, 2015; Salvadó et al., 2016; Vonk et al., 2010). This may lead to selective preservation of
381 terrestrial organic matter in the sediments of the ~~ESAS East-Siberian Arctic Shelf~~ (Karlsson et al. 2011, 2015;
382 Vonk et al. 2010). ~~The proportion of old terrestrial organic matter might also be greater in Arctic sediments due~~
383 ~~to generally low primary production in the area (Stein and Macdonald, 2004).~~ The contribution of topsoil-PF is
384 fairly low throughout the core (3–23 %). This may be due to the location of GC58 between the two major rivers
385 (Kolyma and Indigirka) resulting in relatively low amounts of fluvial inflow depositing topsoil permafrost.

386 To further interpret our results within a larger context of PF-C destabilisation during post-glacial
387 warming, we compared our results with another transgressive deposit collected in the Laptev Sea (PC23, Fig. 1,
388 Tesi et al. 2016a). For the Laptev Sea (PC23), there was a predominant influence of watershed-sourced material
389 via river discharge during the onset of the Holocene, followed by a similar contributions of marine OC and ICD-
390 PF fractions (both sources varying between 31 and 56 %) from ~8,300 cal yrs BP to present. For the ~~East~~
391 ~~Siberian-Sea-ESS~~-(GC58), the contribution of ICD-PF is more prominent for the same time period, indicating a
392 higher significance of coastal erosion for the ~~East-Siberian-SeaESS~~ -compared to the Laptev Sea (Fig. 65).
393 especially when compared to the early Holocene signature. Topsoil-PF fractions in PC23 are slightly higher (8–
394 25 %) than in GC58 (3–23 %) from ~8,300 cal yrs BP to current day. The difference is likely caused by a strong
395 influence of the Lena River at the sampling location of PC23 and less fluvial inflow to GC58 due to its location
396 farther away from the mouths of the Lena, Kolyma and Indigirka rivers.

397 When the shoreline was farther seaward during the early Holocene, the location of the core PC23 from
398 the Laptev Sea experienced a large influence of Lena River derived material (80–90 %) (Tesi et al. 2016a). This
399 material was supplied to the Laptev Sea in response to the deglaciation and associated active-layer deepening in
400 the watershed (Tesi et al. 2016a). Although the record of GC58 does not go back in time to the glacial-
401 interglacial transition at the very onset of the Holocene, ~~our results-we~~ suggest that coastal erosion was likely an

402 | ~~important the dominant~~ process affecting the permafrost carbon supply and deposition also at that time. This
403 | seems ~~possible likely~~, especially when considering the location of the core GC58 in between the rivers, and as
404 | has been observed in modern day shallower sediments in the ~~East Siberian Sea~~ESS (Bröder et al., 2016b; Vonk
405 | et al., 2012).
406

407 | **3.5 Biomarker indications of sSources of terrestrial organic matter**

408 | The lignin fingerprint of organic matter sources in GC58 is consistent with the dual-carbon isotope modelling.
409 | Here we focus on the cinnamyl to vanillyl phenols and syringyl to vanillyl phenols ratios (C/V and S/V,
410 | respectively). The C/V ratio can be used to differentiate between woody (i.e. shrubs and trees) and non-woody
411 | (i.e. leaves, needles, grasses) plant tissues as origin of the terrestrial OC since cinnamyl phenols are produced
412 | only in non-woody vascular plant tissues (Hedges et al., 1988). Moreover, the S/V ratio differentiates between
413 | gymnosperms (conifers) and angiosperms (flowering plants) as syringyl phenols are produced solely in
414 | angiosperms (Hedges et al., 1988). Thereby higher S/V ratios mean more contribution from angiosperm plants.

415 | The S/V and C/V ratios in GC58 show that the terrestrial material transported to the ESS originates
416 | mainly from soft tissue material (i.e. grasses and leaves) both from angiosperm and gymnosperm plants (Fig.
417 | [67](#)). The lignin fingerprint of old Pleistocene material (ICD-PF) is characterised by high ratios of both C/V and
418 | S/V i.e. a high abundance of soft plant tissues from the tundra steppe vegetation (e.g. grass-like material) (Tesi
419 | et al. 2014; Winterfeld et al. 2015). Observations from the Laptev Sea (sediment core PC23, Fig. 1) reveal a
420 | much stronger influence from woody material indicating a watershed source, likely from the Lena River, rather
421 | than from coastal erosion (Fig. [67](#)). It should be noted that the lignin phenols are susceptible to degradation.
422 | Cinnamyl phenols in particular are known to degrade fairly fast, which may lower the C/V ratios (Opsahl and
423 | Benner, 1995). However, even considering degradation effects, the relatively high C/V and S/V values that
424 | characterise GC58, indicate grass-type material typical of tundra/steppe biome and ICD-PF deposits (Tesi et al.,
425 | 2014; Winterfeld et al., 2015).

Formatted: Font: (Default) Times New Roman, 10 pt, Font color: Auto

Formatted: Heading 2

Formatted: Font: (Default) Times New Roman, 10 pt, Font color: Auto

Formatted: Font: (Default) Times New Roman, 10 pt, Not Bold

426 4 Conclusions

427 This down-core study provides new insights into terrestrial carbon dynamics in the ~~East Siberian Sea (ESS)~~
428 from the early Holocene warming period until the present. Our results suggest a high input of terrestrial organic
429 carbon to the ESS during the last glacial-interglacial period caused by permafrost destabilisation. This material
430 was mainly characterised as relict Pleistocene permafrost ~~deposited-released~~ via coastal erosion as a result of the
431 sea level ingression.

432 The flux rates of both lignin and cutin compounds show a declining trend ~~in from~~ the early Holocene
433 ~~until today~~, suggesting a change from mainly terrestrial to marine dominated input. The same change can be
434 seen in the stable carbon isotope ($\delta^{13}\text{C}$) data, which imply a regime shift from terrestrial to more marine
435 dominated sediment input at $\sim 8,400$ cal yrs BP.

436 The source apportionment data highlights the importance of coastal erosion as a terrestrial carbon
437 source to ~~this region of~~ the ESS ~~throughout the Holocene~~. ~~during the Holocene time periods of $\sim 9,500$ – $9,300$ cal~~
438 ~~yrs BP, $\sim 8,500$ – $8,200$ cal yrs BP and from $\sim 1,700$ cal yrs BP to the modern day.~~ This is supported by the lignin
439 composition, which suggests ~~that the terrestrial carbon in the sediment core GC58 consists mainly of a~~
440 ~~deposition of soft tissues of plants (i.e. grasses), typical for tundra/steppe vegetation (i.e., grasses) grown~~ during
441 the Pleistocene. Both the biomarker and grain size data imply that the conditions have been more stable in the
442 ESS in the past $\sim 1,700$ cal yrs BP compared to the early Holocene.

443 The comparison of the source apportionment results ($\delta^{13}\text{C}$, $\Delta^{14}\text{C}$) and the lignin fingerprint (C/V and
444 S/V ratios) for the sediment cores GC58 and PC23 shows a difference in the carbon sources between the ~~East~~
445 ~~Siberian Sea ESS~~ and the adjacent Laptev Sea. The relict Pleistocene permafrost, mostly originating from
446 coastal erosion, may be more dominant in the ESS than in the Laptev Sea. Data for the sediment core PC23
447 show that the Laptev Sea instead had a relatively high input of terrestrial carbon from the watershed, which is
448 likely due to the influence of the Lena River.

449 The accelerating coastal erosion rates along the Siberian coast and amplified warming in the Arctic
450 predicted by many climate models are likely to cause permafrost destabilisation and remobilisation of terrestrial
451 carbon to the marine environment, as observed in the beginning of the Holocene. To better understand the
452 consequences of the permafrost thawing processes, the extent of degradation of terrestrial carbon in the marine
453 environment should be better constrained. Also, to improve the understanding of the processes in the ESS and in
454 the whole Arctic region more historical down-core studies would be needed.

455

456 **Author contributions**

457 T. Tesi and Ö. Gustafsson conceived and designed the research project. T. Tesi, L. Bröder, I. Semiletov, O.
458 Dudarev and Ö. Gustafsson collected the samples with the help from the [IB/RV-1/B Oden](#) crew. C. Pearce and
459 K. Keskitalo developed the age-depth model of GC58. K. Keskitalo carried out all chemical and geological
460 analyses on GC58 and MUC58. M. Sköld and A. Andersson ran the MCMC simulation for the OC source
461 apportionment. A. Andersson estimated the lateral transport times. K. Keskitalo wrote the paper and produced
462 the figures with input from all the co-authors.

463

464 **Competing interests**

465 The authors declare that they have no conflict of interest.

466 **Acknowledgments**

467 | We thank the crew and personnel of [IB/RV_I/B-Oden](#). We thank Rienk Smittenberg for the use of the
468 | microwave extraction facilities. We also thank Carina Jakobsson, Heike Siegmund and Karin Wallner for their
469 | help with the laboratory analyses- [at the Department of Geological Sciences at Stockholm University and at the](#)
470 | [Department of Geology of the Swedish Museum of Natural History](#). This study was supported by the Knut and
471 | Alice Wallenberg Foundation (KAW contract 2011.0027), the Swedish Research Council (VR contract 621-
472 | 2004-4039 and 621-2007-4631), the Nordic Council of Ministers Cryosphere-Climate-Carbon Initiative (project
473 | Defrost, contract 23001) and the European Research Council (ERC-AdG project CC-TOP #695331).
474 | Additionally, I. Semiletov thanks the Russian Government for financial support (mega-grant under contract
475 | #14.Z50.31.0012). O. Dudarev thanks the Russian Science Foundation for financial support (No. 15-17-20032).
476 | T. Tesi acknowledges EU financial support as a Marie Curie fellow (contract no. PIEF-GA-2011-300259).
477 | Contribution no. 1916 of ISMAR-CNR Sede di Bologna. L. Bröder acknowledges financial support from the
478 | Climate Research School of the Bolin Centre for Climate Research. C. Pearce received funding from the Danish
479 | Council for Independent Research / Natural Science (project DFF-4002-00098/FNU). M. Sköld acknowledges
480 | financial support from the Swedish Research Council (Grant 2013:05204). [We also want to thank the editor](#)
481 | [Thomas Cronin and two anonymous reviewers for their insightful comments.](#)

482 **References**

- 483 Alling, V., Porcelli, D., Mörth, C. M., Anderson, L. G., Sanchez-Garcia, L., Gustafsson, Ö., Andersson, P. S.
484 and Humborg, C.: Degradation of terrestrial organic carbon, primary production and out-gassing of CO₂ in the
485 Laptev and East Siberian Seas as inferred from $\delta^{13}\text{C}_{\text{d13C}}$ values of DIC, *Geochim. Cosmochim. Acta*, 95,
486 143–159, doi:10.1016/j.gca.2012.07.028, 2012.
- 487 Amon, R. M. W., Rinehart, A. J., Duan, S., Louchouart, P., Prokushkin, A., Guggenberger, G., Bauch, D.,
488 Stedmon, C., Raymond, P. A., Holmes, R. M., McClelland, J. W., Peterson, B. J., Walker, S. A. and Zhulidov,
489 A. V.: Dissolved organic matter sources in large Arctic rivers, *Geochim. Cosmochim. Acta*, 94, 217–237,
490 doi:10.1016/j.gca.2012.07.015, 2012.
- 491 Ananyev, R., Dmitrevskiy, N., Jakobsson, M., Lobkovsky, L. and Nikiforov, S., [Roslyakov, A. and Semiletov,](#)
492 [I.:](#) Sea-ice ploughmarks in the eastern Laptev Sea, East Siberian Arctic shelf, [Atlas Submar. Glacial Landforms](#)
493 [Mod. Quat. Ancient. Geol. Soc. London. Mem., 46\(1\)](#), 301–302, doi:10.1144/M46.109, 2016.
- 494 [Anderson, L. G., Jutterström, S., Hjalmarsson, S., Wählström, I. and Semiletov, I. P.:](#) Out-gassing of CO₂ from
495 [Siberian Shelf seas by terrestrial organic matter decomposition, *Geophys. Res. Lett.*, 36\(20\),](#)
496 [doi:10.1029/2009GL040046, 2009.](#)
- 497 [Anderson, L. G., Björk, G., Jutterström, S., Pipko, I., Shakhova, N., Semiletov, I. and Wählström, I.:](#) East
498 [Siberian Sea, an Arctic region of very high biogeochemical activity, *Biogeosciences*, 8\(6\), 1745–1754,](#)
499 [doi:10.5194/bg-8-1745-2011, 2011.](#)
- 500 Andersson, A.: A systematic examination of a random sampling strategy for source apportionment calculations,
501 *Sci. Total Environ.*, 412–413, 232–238, doi:10.1016/j.scitotenv.2011.10.031, 2011.
- 502 Andersson, A., Deng, J., Du, K., Zheng, M., Yan, C., Sköld, M. and Gustafsson, Ö.: Regionally-varying
503 combustion sources of the January 2013 severe haze events over eastern China, *Environ. Sci. Technol.*, 49(4),
504 2038–2043, doi:10.1021/es503855e, 2015.
- 505 Barnhart, K. R., Anderson, R. S., Overeem, I., Wobus, C., Clow, G. D. and Urban, F. E.: Modeling erosion of
506 ice-rich permafrost bluffs along the Alaskan Beaufort Sea coast, *J. Geophys. Res. Earth Surf.*, 119(5), 1155–
507 1179, doi:10.1002/2013JF002845, 2014.
- 508 Baskaran, M., Bianchi, T. S. and Filley, T. R.: Inconsistencies between $\delta^{14}\text{C}_{\text{14C}}$ and short-lived radionuclides-
509 based sediment accumulation rates: Effects of long-term remineralization, *J. Environ. Radioact.*, 1–7,
510 doi:10.1016/j.jenvrad.2016.07.028, 2016.
- 511 Bauch, H. a., Kassens, H., Naidina, O. D., Kunz-Pirrung, M. and Thiede, J.: Composition and Flux of Holocene
512 Sediments on the Eastern Laptev Sea Shelf, Arctic Siberia, *Quat. Res.*, 55(3), 344–351,
513 doi:10.1006/qres.2000.2223, 2001a.
- 514 Bauch, H. A., Mueller-Lupp, T., Taldenkova, E., Spielhagen, R. F., Kassens, H., Grootes, P. M., Thiede, J.,
515 Heinemeier, J. and Petryashov, V. V.: Chronology of the holocene transgression at the north siberian margin,
516 *Glob. Planet. Change*, 31(1–4), 125–139, doi:10.1016/S0921-8181(01)00116-3, 2001b.
- 517 [Benner, R. and Opsahl, S.:](#) Early diagenesis of vascular plant tissues: Lignin and cutin decomposition and
518 [biogeochemical implications, 59\(23\), 1995.](#)
- 519 Boudreau, B. P.: Is burial velocity a master parameter for bioturbation?, *Geochim. Cosmochim. Acta*, 58(4),
520 1243–1249, doi:10.1016/0016-7037(94)90378-6, 1994.
- 521 Bröder, L., Tesi, T., Salvadó, J. A., Semiletov, I. P. and Dudarev, O. V. and Gustafsson, Ö.: Fate of
522 terrigenous organic matter across the Laptev Sea from the mouth of the Lena River to the deep sea of the Arctic
523 interior, [Biogeosciences](#), 13(17), 5003–5019, doi:10.5194/bg-13-5003-2016, 2016a.

524 Bröder, L., Tesi, T., Andersson, A., Eglinton, T. I., Semiletov, I. P., Dudarev, O. V., Roos, P. and Gustafsson,
525 Ö.: Historical records of organic matter supply and degradation status in the East Siberian Sea, *Org. Geochem.*,
526 91, 16–30, doi:10.1016/j.orggeochem.2015.10.008, 2016b.

527 Bröder, L., Tesi, T., Andersson, A., Semiletov, I. and Gustafsson, Ö.: Bounding cross-shelf transport time and
528 degradation in land-ocean carbon transfer. 2017. (submitted)

529 Bronk Ramsey, C.: Deposition models for chronological records, *Quat. Sci. Rev.*, 27(1–2), 42–60,
530 doi:10.1016/j.quascirev.2007.01.019, 2008.

531 Bronk Ramsey, C. and Lee, S.: Recent and Planned Developments of the Program OxCal, *Radiocarbon*, 55(2),
532 720–730, doi:10.2458/azu_js_rc.55.16215, 2013.

533 Canuel, E. A. and Martens, C. S.: Reactivity of recently deposited organic matter : near the sediment-water
534 Degradation interface of lipid compounds, *Geochim. Cosmochim. Acta*, 60(10), 1793–1806, 1996.

535 Ciais, P., Gasser, T., Paris, J. D., Caldeira, K., Raupach, M. R., Canadell, J. G., Patwardhan, A., Friedlingstein,
536 P., Piao, S. L. and Gitz, V.: Attributing the increase in atmospheric CO₂ to emitters and absorbers, *Nat. Clim.*
537 *Chang.*, 3(10), 926–930, doi:10.1038/nclimate1942, 2013.

538 Conlan, K. E., Lenihan, H. S., Kvitek, R. G. and Oliver, J. S.: Ice scour disturbance to benthic communities in
539 the Canadian High Arctic, *Mar. Ecol. Prog. Ser.*, 166, 1–16, doi:10.3354/meps166001, 1998.

540 Crichton, K. A., Bouttes, N., Roche, D. M., Chappellaz, J. and Krinner, G.: Permafrost carbon as a missing link
541 to explain CO₂ changes during the last deglaciation, *Nat. Geosci.*, 9(August), 683–686,
542 doi:10.1038/NGEO2793ngeo2793, 2016.

543 [Cronin, T. M., Regan, M. O., Pearce, C., Gemery, L., Toomey, M. and Jakobsson, M.: Deglacial sea-level
544 history of the East Siberian Sea Margin, \(March\), doi:10.5194/cp-2017-19, 2017.](#)

545 Elmquist, M., Zencak, Z. and Gustafsson, Ö.: A 700 year sediment record of black carbon and polycyclic
546 aromatic hydrocarbons near the EMEP air monitoring station in Aspveten, Sweden, *Environ. Sci. Technol.*,
547 41(20), 6926–6932, doi:10.1021/es070546m, 2007.

548 Farella, N., Lucotte, M., Louchouart, P. and Roulet, M.: Deforestation modifying terrestrial organic transport
549 , Brazilian Amazon in the Rio Tapajo, *Org. Geochem.*, 32, 1443–1458, 2001.

550 [Fisher, D., Dyke, A., Koerner, R., Bourgeois, J., Kinnard, C., Zdanowicz, C., de Vernal, A., Hillaire-Marcel, C.,
551 Savelle, J. and Rochon, A.: Natural Variability of Arctic Sea Ice Over the Holocene, *Eos, Trans. Am. Geophys.*
552 *Union*, 87\(28\), 273–275, 2006.](#)

553 Fry, B. and Sherr, E. B.: δ¹³C Measurements as indicators of carbon flow in marine and freshwater ecosystems,
554 *Contrib. Mar. Sci.*, 27, 13–49, 1984.

555 Goñi, M. A. and Hedges, J. I.: Sources and reactivities of marine-derived organic matter in coastal sediments as
556 determined by alkaline CuO oxidation, *Geochim. Cosmochim. Acta*, 59(14), 2965–2981, doi:10.1016/0016-
557 7037(95)00188-3, 1995.

558 Goñi, M. A. and Montgomery, S.: Alkaline CuO oxidation with a microwave digestion system: Lignin analyses
559 of geochemical samples, *Anal. Chem.*, 72(14), 3116–3121, doi:10.1021/ac991316w, 2000.

560 [Goñi, M. A., Nelson, B., Blanchette, R. A. and Hedges, J. I.: Fungal degradation of wood lignins: Geochemical
561 perspectives from CuO-derived phenolic dimers and monomers, *Geochim. Cosmochim. Acta*, 57\(16\), 3985–
562 4002, doi:10.1016/0016-7037\(93\)90348-Z, 1993.](#)

563 Goñi, M. A., Yunker, M. B., MacDonald, R. W. and Eglinton, T. I.: Distribution and sources of organic
564 biomarkers in arctic sediments from the Mackenzie River and Beaufort Shelf, *Mar. Chem.*, 71(1–2), 23–51,
565 doi:10.1016/S0304-4203(00)00037-2, 2000.

566 [Goñi, M. A., O'Connor, A. E., Kuzyk, Z. Z., Yunker, M. B., Gobeil, C. and Maedonald, R. W.: Distribution and](#)
567 [sources of organic matter in surface marine sediments across the North American Arctic margin, *J. Geophys.*](#)
568 [Res. Ocean., 118, 4017–4035, doi:10.1002/jgre.20286, 2013.](#)

569 Gordeev, V. V.: Fluvial sediment flux to the Arctic Ocean, *Geomorphology*, 80(1–2), 94–104,
570 doi:10.1016/j.geomorph.2005.09.008, 2006.

571 Grigoriev, M.: Coastal sediment and organic carbon flux to the Laptev and East Siberian Seas, , 12, 8763, 2010.

572 [Grigoriev, M. N. and Rachold, V.:](#) The degradation of coastal permafrost and the organic carbon balance of the
573 [Laptev and East Siberian Seas, ~~-\(1987\);~~Permafr. Proc. 8th Int. Conf. Permafrost, 21-25 July 2003, Zurich,](#)
574 [Switz.. \(1987\), 319–324, 2003.](#)

575 Günther, F., Overduin, P. P., Yakshina, I. A., Opel, T., Baranskaya, A. V. and Grigoriev, M. N.: Observing
576 Muostakh disappear: Permafrost thaw subsidence and erosion of a ground-ice-rich Island in response to arctic
577 summer warming and sea ice reduction, *Cryosphere*, 9(1), 151–178, doi:10.5194/tc-9-151-2015, 2015.

578 Hartnett, H., Keil, R., Hedges, J. and Devol, A.: Influence of oxygen exposure time on organic carbon
579 preservation in continental margin sediments, *Nature*, 391(February), 572–575, doi:10.1038/35351, 1998.

580 Hedges, J. I., Blanchette, R. A., Weliky, K. and Devol, A. H.: Effects of fungal degradation on the CuO
581 oxidation products of lignin: A controlled laboratory study, *Geochim. Cosmochim. Acta*, 52(11), 2717–2726,
582 doi:10.1016/0016-7037(88)90040-3, 1988.

583 Higuchi, T.: Formation and biological degradation of lignins, *Adv Enzym. Relat Areas Mol Biol*, 34, 207–283,
584 1971.

585 Hilton, R. G., Galy, V., Gaillardet, J., Dellinger, M., Bryant, C., O'Regan, M., Gröcke, D. R., Coxall, H.,
586 Bouchez, J. and Calmels, D.: Erosion of organic carbon in the Arctic as a geological carbon dioxide sink,
587 *Nature*, 524(7563), 84–87, doi:10.1038/nature14653, 2015.

588 Hugelius, G., Strauss, J., Zubrzycki, S., Harden, J. W., Schuur, E. A. G., Ping, C. L., Schirmermeister, L., Grosse,
589 G., Michaelson, G. J., Koven, C. D., O'Donnell, J. A., Elberling, B., Mishra, U., Camill, P., Yu, Z., Palmtag, J.
590 and Kuhry, P.: Estimated stocks of circumpolar permafrost carbon with quantified uncertainty ranges and
591 identified data gaps, *Biogeosciences*, 11(23), 6573–6593, doi:10.5194/bg-11-6573-2014, 2014.

592 IPCC Working Group I, I., Stocker, T. F., Qin, D., Plattner, G.-K., Tignor, M., Allen, S. K., Boschung, J.,
593 Nauels, A., Xia, Y., Bex, V. and Midgley, P. M.: IPCC, 2013: Climate Change 2013: The Physical Science
594 Basis. Contribution of Working Group I to the Fifth Assessment Report of the Intergovernmental Panel on
595 Climate Change, IPCC, AR5, 1535, 2013.

596 Jakobsson, M.: Hypsometry and volume of the Arctic Ocean and its constituent seas, *Geochemistry Geophys.*
597 *Geosystems*, 3(5), 1–18, 2002.

598 Jakobsson, M., Andreassen, K., Bjarnadóttir, L. R., Dove, D., Dowdeswell, J. A., England, J. H., Funder, S.,
599 Hogan, K., Ingólfsson, Ó., Jennings, A., Krog Larsen, N., Kirchner, N., Landvik, J. Y., Mayer, L., Mikkelsen,
600 N., Möller, P., Niessen, F., Nilsson, J., O'Regan, M., Polyak, L., Nørgaard-Pedersen, N. and Stein, R.: Arctic
601 Ocean glacial history, *Quat. Sci. Rev.*, 92, 40–67, doi:10.1016/j.quascirev.2013.07.033, 2014.

602 Jones, B. M., Arp, C. D., Jorgenson, M. T., Hinkel, K. M., Schmutz, J. A. and Flint, P. L.: Increase in the rate
603 and uniformity of coastline erosion in Arctic Alaska, *Geophys. Res. Lett.*, 36(3), 1–5,
604 doi:10.1029/2008GL036205, 2009.

605 Kanevskiy, M., Shur, Y., Strauss, J., Jorgenson, T., Fortier, D., Stephani, E. and Vasiliev, A.: Patterns and rates
606 of riverbank erosion involving ice-rich permafrost (yedoma) in northern Alaska, *Geomorphology*, 253, 370–
607 384, doi:10.1016/j.geomorph.2015.10.023, 2016.

608 Karlsson, E., Gelting, J., Tesi, T., Dongen, B., Andersson, A., Semiletov, I., Charkin, A., Dudarev, O. and
609 Gustafsson, Ö.: Different sources and degradation state of dissolved, particulate, and sedimentary organic matter
610 along the Eurasian Arctic coastal margin, *Global Biogeochem. Cycles*, (30), 898–919,
611 doi:doi:10.1002/2015GB005307, 2016.

612 Karlsson, E. S., Charkin, A., Dudarev, O., Semiletov, I., Vonk, J. E., [Sánchez-García, L.](#), Andersson, A. and
613 Gustafsson, ~~Ö.~~ [and Aretie, I.](#): Carbon isotopes and lipid biomarker investigation of sources-, transport and
614 degradation of terrestrial organic matter in the Buor-Khaya Bay, SE Laptev Sea, *Biogeosciences*, **8(7)**, 1865–
615 1879, doi:10.5194/bg-8-1865-2011, 2011.

616 Karlsson, E. S., Brüchert, V., Tesi, T., Charkin, A., Dudarev, O., Semiletov, I. and Gustafsson, Ö.: Contrasting
617 regimes for organic matter degradation in the East Siberian Sea and the Laptev Sea assessed through microbial
618 incubations and molecular markers, *Mar. Chem.*, 170, 11–22, doi:10.1016/j.marchem.2014.12.005, 2015.

619 [Kaufman, D. S., Ager, T. A., Anderson, N. J., Anderson, P. M., Andrews, J. T., Bartlein, P. J., Brubaker, L. B.,](#)
620 [Coats, L. L., Cwynar, L. C., Duvall, M. L., Dyke, A. S., Edwards, M. E., Eisner, W. R., Gajewski, K.,](#)
621 [Geirsdóttir, A., Hu, F. S., Jennings, A. E., Kaplan, M. R., Kerwin, M. W., Lozhkin, A. V., MacDonald, G. M.,](#)
622 [Miller, G. H., Mock, C. J., Oswald, W. W., Otto-Bliesner, B. L., Porinchu, D. F., Rühland, K., Smol, J. P., Steig,](#)
623 [E. J. and Wolfe, B. B.: Holocene thermal maximum in the western Arctic \(0-180??W\). *Quat. Sci. Rev.*, **23\(5–6\)**,](#)
624 [529–560. doi:10.1016/j.quascirev.2003.09.007, 2004.](#)

625 Keil, R. G., Dickens, A. F., Arnarson, T., Nunn, B. L. and Devol, A. H.: What is the oxygen exposure time of
626 laterally transported organic matter along the Washington margin?, *Mar. Chem.*, 92(1–4 SPEC. ISS.), 157–165,
627 doi:10.1016/j.marchem.2004.06.024, 2004.

628 Kohlbach, D., Graeve, M., A. Lange, B., David, C., Peeken, I. and Flores, H.: The importance of ice algae-
629 produced carbon in the central Arctic Ocean ecosystem: Food web relationships revealed by lipid and stable
630 isotope analyses, *Limnol. Oceanogr.*, 61(6), 2027–2044, doi:10.1002/lno.10351, 2016.

631 Koven, C. D., Ringeval, B., Friedlingstein, P., Ciais, P., Cadule, P. and ~~Khvorostyanov, D.~~ [Krunner, G. and](#)
632 [Tarnocai, C.](#): Permafrost carbon-climate feedbacks accelerate global warming, ~~(45)~~ *Proc. Natl. Acad. Sci.*,
633 [108\(36\), 14769–14774.](#) doi:10.1073/pnas.1103910108, 2011.

634 Kunst, L. and Samuels, A. L.: Biosynthesis and secretion of plant cuticular wax, *Prog. Lipid Res.*, 42(1), 51–80,
635 doi:10.1016/S0163-7827(02)00045-0, 2003.

636 [Köhler, P., Knorr, G. and Bard, E.: Permafrost thawing as a possible source of abrupt carbon release at the onset](#)
637 [of the Bølling/Allerød. *Nat. Clim. Chang.*, doi:10.1038/ncomms6520, 2014.](#)

638 Lambeck, K., Rouby, H., Purcell, A., Sun, Y. and Sambridge, M.: Sea level and global ice volumes from the
639 Last Glacial Maximum to the Holocene., *Proc. Natl. Acad. Sci. U. S. A.*, 111(43), 15296–~~303~~15303,
640 doi:10.1073/pnas.1411762111, 2014.

641 Louchouart, P., Lucotte, M. and Farella, N.: Historical and geographical variations of sources and transport of
642 terrigenous organic matter within a large-scale coastal environment, *Org. Geochem.*, 30(7), 675–699,
643 doi:10.1016/S0146-6380(99)00019-4, 1999.

644 McClelland, J. W., Holmes, R. M., Peterson, B. J., Raymond, P. A., Striegl, R. G., Zhulidov, A. V., Zimov, S.
645 A., Zimov, N., Tank, S. E., Spencer, R. G. M., Staples, R., Gurtovaya, T. Y. and Griffin, C. G.: Particulate
646 organic carbon and nitrogen export from major Arctic rivers, *Global Biogeochem. Cycles*, doi:10.1002/
647 2015GB005351, 2016.

648 Mueller-Lupp, T., Bauch, H. A., Erlenkeuser, H., Hefter, J., Kassens, H. and Thiede, J.: Changes in the
649 deposition of terrestrial organic matter on the Laptev Sea shelf during the Holocene: evidence from stable

Formatted: English (U.K.)

650 carbon isotopes, *Int. J. Earth Sci.*, 89(3), 563–568, doi:10.1007/s005310000128, 2000.

651 Olefeldt, D., Goswami, S., Grosse, G., Hayes, D., Hugelius, G., Kuhry, P., McGuire, A. D., Romanovsky, V. E.,
652 Sannel, A. B. K., Schuur, E. A. G. and Turetsky, M. R.: Circumpolar distribution and carbon storage of
653 thermokarst landscapes, *Nat. Commun.*, 7, 13043, doi:10.1038/ncomms13043, 2016.

654 [Opsahl, S. and Benner, R.: Early diagenesis of vascular plant tissues: Lignin and cutin decomposition and
655 biogeochemical implications, *Geochim. Cosmochim. Acta*, 59\(23\), 4889–4904, doi:10.1016/0016-
656 7037\(95\)00348-7, 1995.](#)

657 Parnell, A. C., Phillips, D. L., Bearhop, S., Semmens, B. X., Ward, E. J., Moore, J. W., Jackson, A. L., [Grey, J.,
658 Kelly, D. J.](#) and Inger, R.: Bayesian Stable Isotope Mixing Models, [arXiv Prepr. arXiv:1601.00016](#), *16, Environmetrics*,
659 [24\(6\), 387–399, doi:10.1002/env.2221, 20122013.](#)

660 Pearson, A., McNichol, A. P., Schneider, R. J., Von Reden, K. F. and Zheng, Y.: Microscale AMS 14C
661 measurements at NOSAMS, *Radiocarbon*, 40(1), 61–75, 1998.

662 Prah, F. G., Ertel, J. R., Goni, M. A., Sparrow, M. A. and Eversmeyer, B.: Terrestrial organic carbon
663 contributions to sediments on the Washington margin, *Geochim. Cosmochim. Acta*, 58(14), 3035–3048,
664 doi:10.1016/0016-7037(94)90177-5, 1994.

665 [Reimer, P. J., Bard, E., Bayliss, A., Beck, J. W., Blackwell, P. G., Ramsey, C. B., Buck, C. E., Cheng, H.,
666 Edwards, R. L., Friedrich, M., Grootes, P. M., Guilderson, T. P., Haflidason, H., Hajdas, L., Hatté, C., Heaton, T.
667 J., Hoffmann, D. L., Hogg, A. G., Hughen, K. A., Kaiser, K. F., Kromer, B., Manning, S. W., Niu, M., Reimer,
668 R. W., Richards, D. A., Scott, E. M., Southon, J. R., Staff, R. A., Turney, C. S. M. and van der Plicht, J.:
669 *IntCal13 and Marine13 Radiocarbon Age Calibration Curves 0–50,000 Years cal BP, Radiocarbon*, 55\(4\),
670 1869–1887, doi:10.2458/azu_js_rc.55.16947, 2013.](#)

671 Romanovskii, N. N., Hubberten, H. W., Gavrillov, A. V., Tumskoy, V. E. and Kholodov, A. L.: Permafrost of the
672 east Siberian Arctic shelf and coastal lowlands, in *Quaternary Science Reviews*, vol. *Quat. Sci. Rev.*, 23, pp. (11–
673 13), 1359–1369, doi:10.1016/j.quascirev.2003.12.014, 2004.

674 Salvadó, J. A., Tesi, T., Sundbom, M., Karlsson, E., Kruså, M., Semiletov, I. P., Panova, E. and Gustafsson, Ö.:
675 Contrasting composition of terrigenous organic matter in the dissolved, particulate and sedimentary organic
676 carbon pools on the outer East Siberian Arctic Shelf, *Biogeosciences*, 13(22), 6121–6138, doi:10.5194/bg-13-
677 6121-2016, 2016.

678 Sánchez-García, L., Alling, V., Pugach, S., Vonk, J., Van Dongen, B., Humborg, C., Dudarev, O., Semiletov, I.
679 and Gustafsson, Ö.: Inventories and behavior of particulate organic carbon in the Laptev and East Siberian seas,
680 *Global Biogeochem. Cycles*, 25(2), 1–13, doi:10.1029/2010GB003862, 2011.

681 Schirrmeister, L., Kunitsky, V., Grosse, G., Wetterich, S., Meyer, H., Schwamborn, G., Babiy, O., Derevyagin,
682 A. and Siegert, C.: Sedimentary characteristics and origin of the Late Pleistocene Ice Complex on north-east
683 Siberian Arctic coastal lowlands and islands - A review, *Quat. Int.*, 241(1–2), 3–25,
684 doi:10.1016/j.quaint.2010.04.004, 2011.

685 Schuur, E. A. G., McGuire, A. D., Grosse, G., Harden, J. W., Hayes, D. J., Hugelius, G., Koven, C. D. and
686 Kuhry, P.: Climate change and the permafrost carbon feedback, *Nature*, 520(January 2016), 171–179,
687 doi:10.1038/nature14338, 2015.

688 Semiletov, I., Dudarev, O., Luchin, V., Charkin, A., Shin, K. H. and Tanaka, N.: The East Siberian Sea as a
689 transition zone between Pacific-derived waters and Arctic shelf waters, *Geophys. Res. Lett.*, 32(10), 1–5,
690 doi:10.1029/2005GL022490, 2005.

691 [Semiletov, I., Pipko, I., Gustafsson, Ö., Anderson, L. G., Sergienko, V., Pugach, S., Dudarev, O., Charkin, A.,](#)

692 [Gukov, A., Bröder, L., Andersson, A., Spivak, E. and Shakhova, N.: Acidification of East Siberian Arctic Shelf](#)
693 [waters through addition of freshwater and terrestrial carbon, *Nat. Geosci.*, 9\(April\), 361–365,](#)
694 [doi:10.1038/NEGO2695, 2016.](#)

695 Semiletov, I. P.: Aquatic Sources and Sinks of CO₂ and CH₄ in the Polar Regions, *J. Atmos. Sci.*, 56, 1999a.
696 Semiletov, I. P.: Destruction of the coastal permafrost ground as an important factor in biogeochemistry of the
697 Arctic Shelf waters, *Trans. [Doklady] Russ. Acad. Sci.*, 368(6), 679–682, 1999b.

698 Semiletov, I. P., Pipko, I. I., Shakhova, N. E., Dudarev, O. V., Pugach, S. P., Charkin, A. N., Mcroy, C. P.,
699 Kosmach, D. and Gustafsson, Ö.: Carbon transport by the Lena River from its headwaters to the Arctic Ocean,
700 with emphasis on fluvial input of terrestrial particulate organic carbon vs. carbon transport by coastal erosion,
701 *Biogeosciences*, 8(9), 2407–2426, doi:10.5194/bg-8-2407-2011, 2011.

702 [Semiletov, I. P., Shakhova, N. E., Sergienko, V. I., Pipko, I. I. and Dudarev, O. V.: On carbon transport and fate](#)
703 [in the East Siberian Arctic land–shelf–atmosphere system, *Environ. Res. Lett.*, 7\(1\), 15201, doi:10.1088/1748-](#)
704 [9326/7/1/015201, 2012.](#)

705 Semiletov, I. P., Shakhova, N. E., Pipko, I. I., Pugach, S. P., Charkin, A. N., Dudarev, O. V., Kosmach, D. A.
706 and Nishino, S.: Space-time dynamics of carbon and environmental parameters related to carbon dioxide
707 emissions in the Buor-Khaya Bay and adjacent part of the Laptev Sea, *Biogeosciences*, 10(9), 5977–5996,
708 doi:10.5194/bg-10-5977-2013, 2013.

709 [Shakhova, N., Semiletov, I., Leifer, I., Salyuk, A., Rekant, P. and Kosmach, D.: Geochemical and geophysical](#)
710 [evidence of methane release over the East Siberian Arctic Shelf, *J. Geophys. Res. Ocean.*, 115\(8\), 1–14,](#)
711 [doi:10.1029/2009JC005602, 2010.](#)

712 [Shakhova, N., Semiletov, I., Leifer, I., Sergienko, V., Salyuk, A., Kosmach, D., Chernykh, D., Stubbs, C.,](#)
713 [Nicolsky, D., Tumskey, V. and Gustafsson, Ö.: Ebullition and storm-induced methane release from the East](#)
714 [Siberian Arctic Shelf, *Nat. Geosci.*, 7\(January\), 64–70, doi:10.1038/ngeo2007, 2013.](#)

715 [Shakhova, N., Semiletov, I., Sergienko, V., Lobkovsky, L., Yusupov, V., Salyuk, A., Salomatin, A., Chernykh,](#)
716 [D., Kosmach, D., Panteleev, G., Nicolsky, D., Samarkin, V., Joye, S., Charkin, A., Dudarev, O., Meluzov, A.](#)
717 [and Gustafsson, Ö.: The East Siberian Arctic Shelf: Towards further assessment of permafrost-related methane](#)
718 [fluxes and role of sea ice, *Philos. Trans. R. Soc. A*, 373\(2052\), 20140451, doi:10.1098/rsta.2014.0451, 2015.](#)

719 [Shakhova, N. E., Sergienko, V. I. and Semiletov, I. P.: The contribution of the East Siberian shelf to the modern](#)
720 [methane cycle, *Her. Russ. Acad. Sci.*, 79\(3\), 237–246, doi:10.1134/S101933160903006X, 2009.](#)

721 [Smith, S. L., Henrichs, S. M. and Rho, T.: Stable C and N isotopic composition of sinking particles and](#)
722 [zooplankton over the southeastern Bering Sea shelf, . 49, 6031–6050, 2002.](#)

723 [Stanford, J. D., Hemingway, R., Rohling, E. J., Challenor, P. G., Medina-elizalde, M. and Lester, A. J.: Sea-](#)
724 [level probability for the last deglaciation : A statistical analysis of far- field records, *Glob. Planet. Change*, 1–11,](#)
725 [doi:10.1016/j.gloplacha.2010.11.002, 2010.](#)

726 Stein, R. and Macdonald, R. W.: The organic carbon cycle in the Arctic Ocean., 2004.

727 Stuiver, M. and Braziunas, T. F.: Modeling Atmospheric ¹⁴C Influences and ¹⁴C Ages of Marine Samples to
728 10,000 BC, *Radiocarbon*, 35(1), 137–189, doi:10.1017/S0033822200013874, 1993.

729 Stuiver, M. and Polach, H. a: *Radiocarbon*, *Radiocarbon*, 19(3), 355–363, doi:10.1021/ac100494m, 1977.

730 Tamocai, C., Canadell, J. G., Schuur, E. A. G., Kuhry, P., Mazhitova, G. and Zimov, S.: Soil organic carbon
731 pools in the northern circumpolar permafrost region, *Global Biogeochem. Cycles*, 23(2), 1–11,
732 doi:10.1029/2008GB003327, 2009.

733 Tesi, T., Semiletov, I., Hugelius, G., Dudarev, O., Kuhry, P. and Gustafsson, Ö.: Composition and fate of

734 terrigenous organic matter along the Arctic land-ocean continuum in East Siberia: Insights from biomarkers and
735 carbon isotopes, *Geochim. Cosmochim. Acta*, 133, 235–256, doi:10.1016/j.gca.2014.02.045, 2014.

736 Tesi, T., Muschitiello, F., Smittenberg, R. H., Jakobsson, M., Vonk, J. E., Hill, P., Andersson, A., Kirchner, N.,
737 Noormets, R., Dudarev, O., Semiletov, I. and Gustafsson, Ö.: Massive remobilization of permafrost carbon
738 during post-glacial warming, *Nat. Commun.*, 7, 13653, doi:10.1038/ncomms13653, 2016a.

739 Tesi, T., Semiletov, I. P., Dudarev, O. V., Andersson, A. and Gustafsson, Ö.: Matrix association effects on
740 hydrodynamic sorting and degradation of terrestrial organic matter during cross-shelf transport in the Laptev
741 and East Siberian shelf seas, *J. Geophys. Res. Biogeosciences*, 121(3), 731–752,
742 doi:10.1002/2015JG003067. ~~Received~~, 2016b.

743 Vetrov, A. and Romankevich, E.: Carbon Cycle in the Russian Arctic Seas, Springer-Verlag Berlin Heidelberg.,
744 ~~331 p.~~ doi:10.1007/978-3-662-06208-1, 2004.

745 Vonk, J. E. and Gustafsson, Ö.: Permafrost-carbon complexities, *Nat. Geosci.*, 6(9), 675–676,
746 doi:10.1038/ngeo1937, 2013.

747 Vonk, J. E., Sánchez-García, L., Semiletov, I., Dudarev, O., Eglinton, T., Andersson, A. and Gustafsson, O.:
748 Molecular and radiocarbon constraints on sources and degradation of terrestrial organic carbon along the
749 Kolyma paleoriver transect, East Siberian Sea, *Biogeosciences*, 7(10), 3153–3166, doi:10.5194/bg-7-3153-2010,
750 2010.

751 Vonk, J. E., Sánchez-García, L., van Dongen, B. E., Alling, V., Kosmach, D., Charkin, a., Semiletov, I. P.,
752 Dudarev, O. V., Shakhova, N., Roos, P., Eglinton, T. I., Andersson, a. and Gustafsson, Ö.: Activation of old
753 carbon by erosion of coastal and subsea permafrost in Arctic Siberia, *Nature*, 489(7414), 137–140,
754 doi:10.1038/nature11392, 2012.

755 ~~Vonk, J. E., Semiletov, I., Dudarev, O., Eglinton, T. I., Andersson, A., Shakhova, N., Charkin, A., Heim, B. and~~
756 ~~Gustafsson, Ö.: Preferential burial of permafrost derived organic carbon in Siberian Arctic shelf waters, *J.*~~
757 ~~*Geophys. Res. Ocean.*, 8410–8421, doi:10.1002/2014JC010261, 2014.~~

758 Winterfeld, M., Goñi, M. A., Just, J., Hefter, J. and Mollenhauer, G.: Characterization of particulate organic
759 matter in the Lena River delta and adjacent nearshore zone , NE Siberia – Part 2 : Lignin-derived phenol
760 compositions, , 2261–2283, doi:10.5194/bg-12-2261-2015, ~~2015a~~2015.

761 ~~Winterfeld, M., Laepple, T. and Mollenhauer, G.: Characterization of particulate organic matter in the Lena~~
762 ~~River delta and adjacent nearshore zone , NE Siberia—Part I - Radiocarbon inventories, , 3769–3788,~~
763 ~~doi:10.5194/bg-12-3769-2015, 2015b.~~

764

765 Figures and captions

766

767 Table 1. Radiocarbon (¹⁴C) ages of the mollusc shells retrieved from the sediment core GC58. The ¹⁴C ages are
 768 shown in years BP with an age error (yrs) and as calibrated ¹⁴C ages (cal yrs BP) with ~~two~~ standard deviations
 769 ($\pm 2\sigma$) of the individual ¹⁴C dates. The calibration curve used was Marine13 (Reimer et al., 2013) and a ΔR value of
 770 50 ± 100 yrs (Bauch et al., 2001a). Also shown the $\delta^{13}\text{C}$ (‰) values of the mollusc shells.

Corrected depth* (cm)	NOSAMS Accession nr.	Type	Age ¹⁴ C (yrs BP)	Age error (yrs)	$\delta^{13}\text{C}$ (‰)	Age ¹⁴ C	Age ¹⁴ C	2σ
						(Cal yrs BP) <u>median</u>	(Cal yrs BP) <u>mean</u>	
3.5	OS-119395	Mollusc <u>shell</u> , fragments	895	25	0.55	<u>462</u>	455	<u>92184</u>
8.5	OS-120688	Mollusc <u>shell</u> , fragments	>Modern	-	1.70	<u>39</u>	45	<u>3264</u>
34.5	OS-120689	Mollusc <u>shell</u> , fragments	2,260	20	1.55	<u>1,807</u>	1,806	<u>+25250</u>
39.5	OS-120690	Mollusc <u>shell</u> , fragments	2,210	15	1.55	<u>1,748</u>	1,746	<u>+22244</u>
47.5	OS-123161	Mollusc <u>shell</u> , fragments	7,960	35	0.90	<u>8,372</u>	8,372	<u>+10220</u>
51.5	OS-119396	Mollusc <u>shell</u> , fragments	8,010	25	1.06	<u>8,426</u>	8,429	<u>+12224</u>
54.5	OS-120691	Mollusc <u>shell</u> , fragments	8,020	20	0.49	<u>8,437</u>	8,441	<u>+13226</u>
65.5	OS-119397	Mollusc <u>shell</u> , <i>Macoma calcareo</i>	8,780	25	-2.46	<u>9,384</u>	9,372	<u>+17234</u>
72.5	OS-120692	Mollusc <u>shell</u> , fragments	8,880	20	-0.91	<u>9,493</u>	9,499	<u>+22244</u>
78.5	OS-120693	Mollusc <u>shell</u> , fragments	8,950	25	-0.79	<u>9,579</u>	9,595	<u>+32264</u>

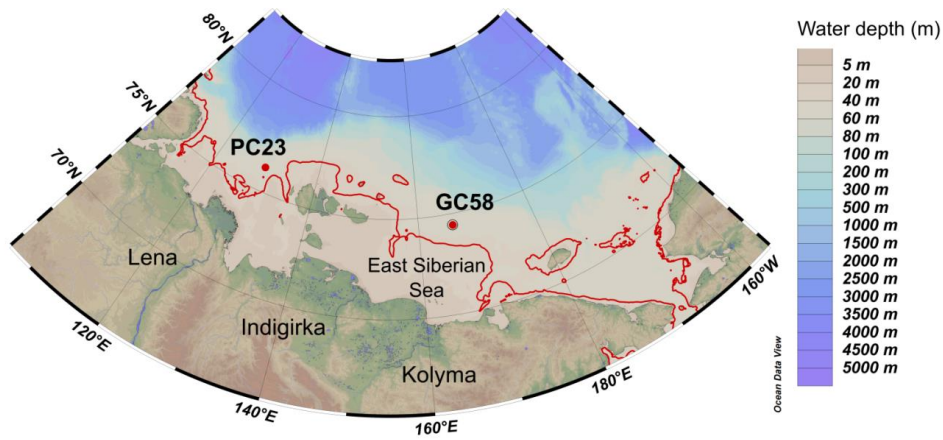
Field Code Changed

Formatted: Font: Bold

Formatted Table

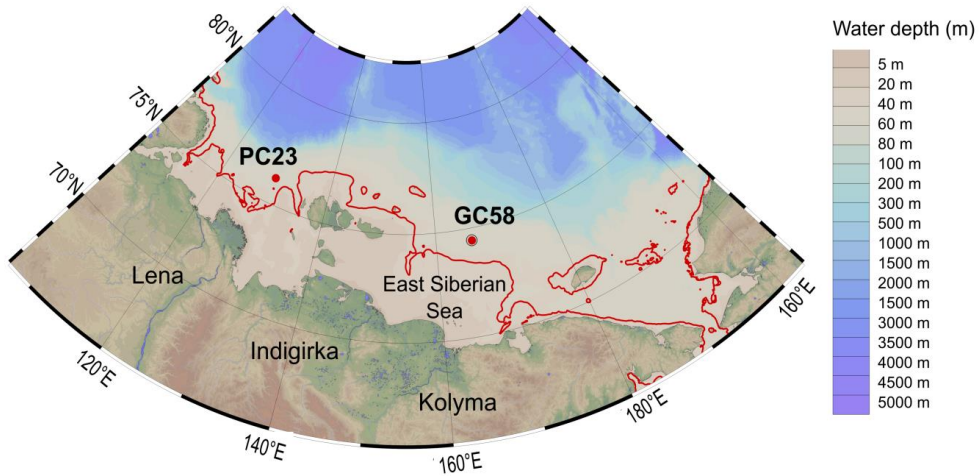
771 *Corrected depth is the original depth + 3 cm to account for core top loss during sampling (Sect 2.4).

772



Formatted: Font: (Default) Times New Roman

773

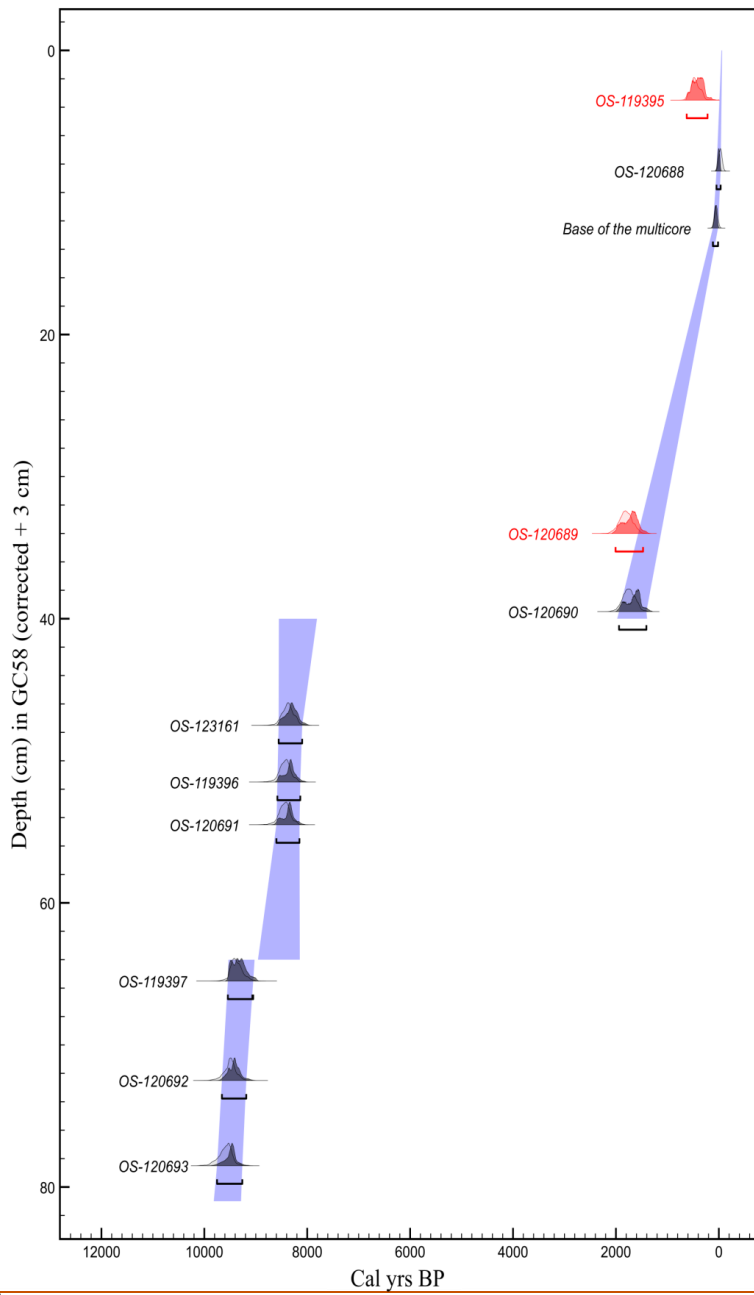


Formatted: Font: (Default) Times New Roman

774

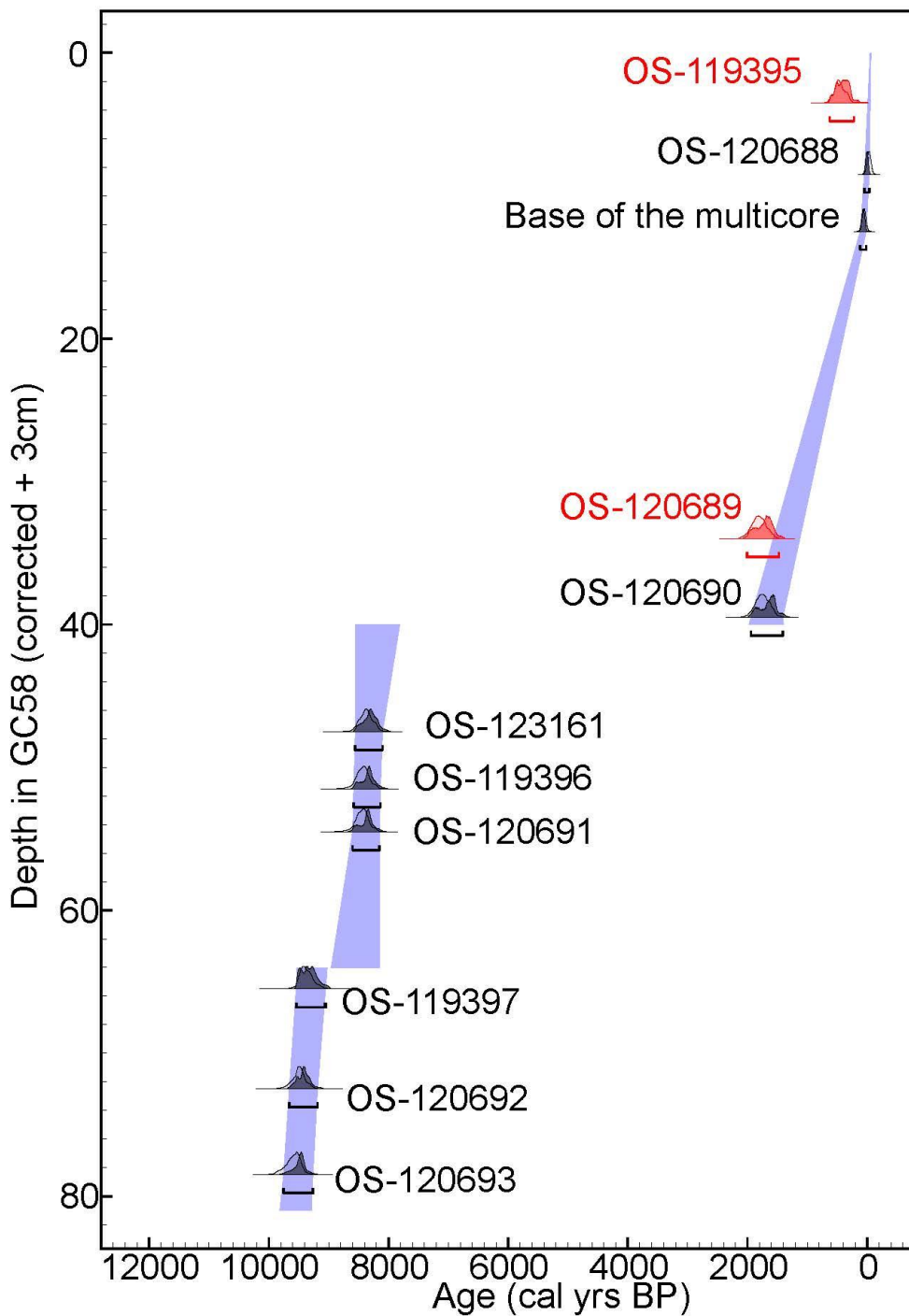
775 **Figure 1.** Map of the Eastern Siberian Arctic Shelf showing the location of the sampling site (Station SWERUS C3-1-
 776 58) (Schlitzer, R., Ocean Data View, <http://odv.awi.de>, 2015). Also shown in the map is the location of the sediment
 777 core PC23 (Station SWERUS C3-1-23, Tesi et al., 2016a). The red line marks the isobath (34 m water depth) which is
 778 approximately where the coast line was in the beginning of the sediment archive (GC58) ~9,500 cal yrs BP (Lambeck
 779 et al., 2014).

780



Formatted: Font: (Default) Times New Roman, 9 pt, Bold

Formatted: Left



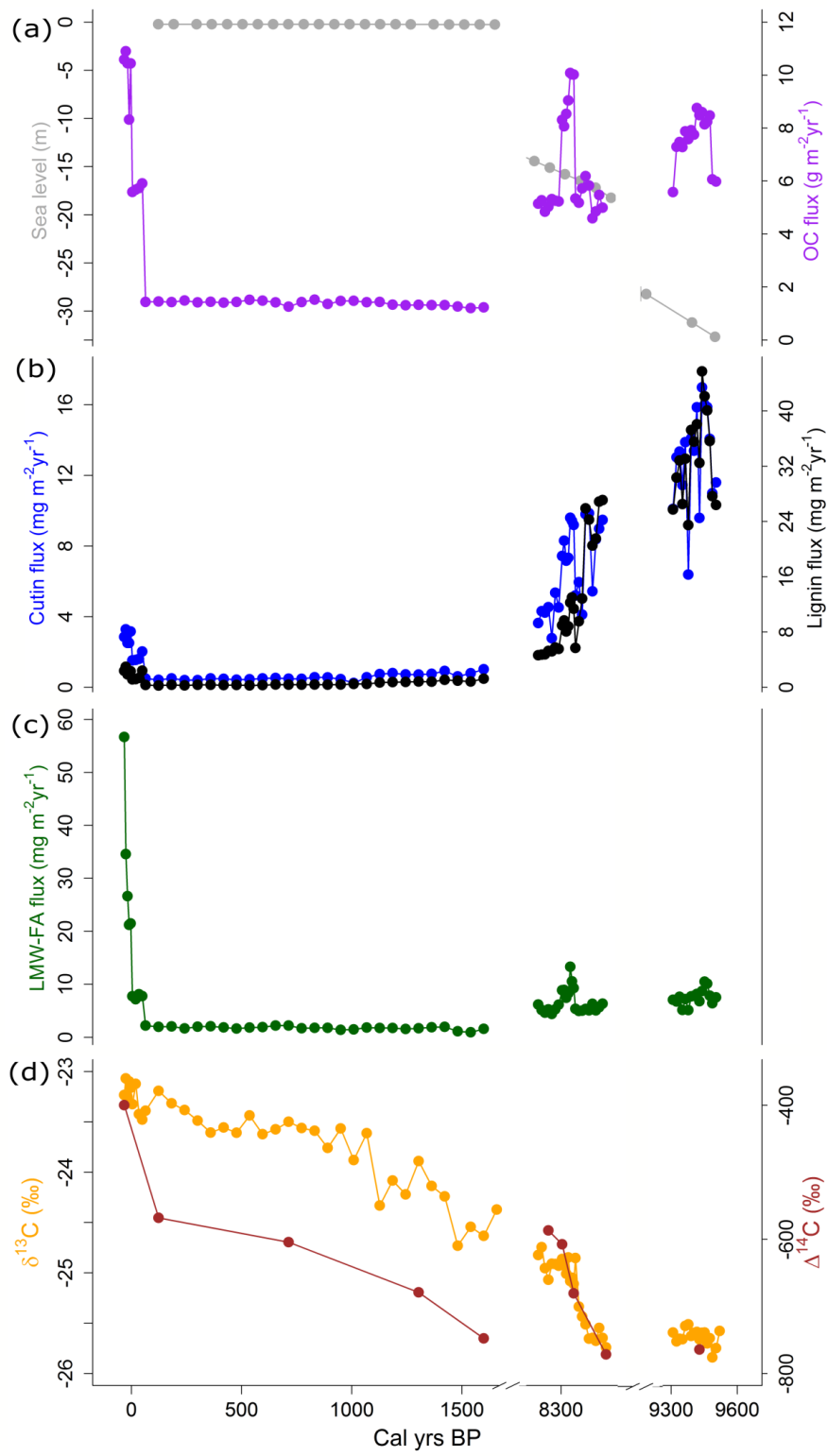
Formatted: Font: (Default) Times New Roman, 9 pt, Bold

784
 785 Figure 2. An age-depth model of the sediment core GC58 based on radiocarbon (^{14}C) dated molluscs shells (see Table
 786 1) and ^{210}Pb (base of a multicore collected at the same location, see Supplementary Information Table S2). All the
 787 modelled dates were calibrated with Marine13 calibration curve (Reimer et al., 2013). A ΔR value of 50 ± 100 yrs was
 788 used to account for the differences in the local reservoir age based on (Bauch et al., 2001a). The core GC58 dates back
 789 $\sim 9,500$ cal yrs BP. The calibrated age probability distributions are plotted for each radiocarbon date in grey. Outliers

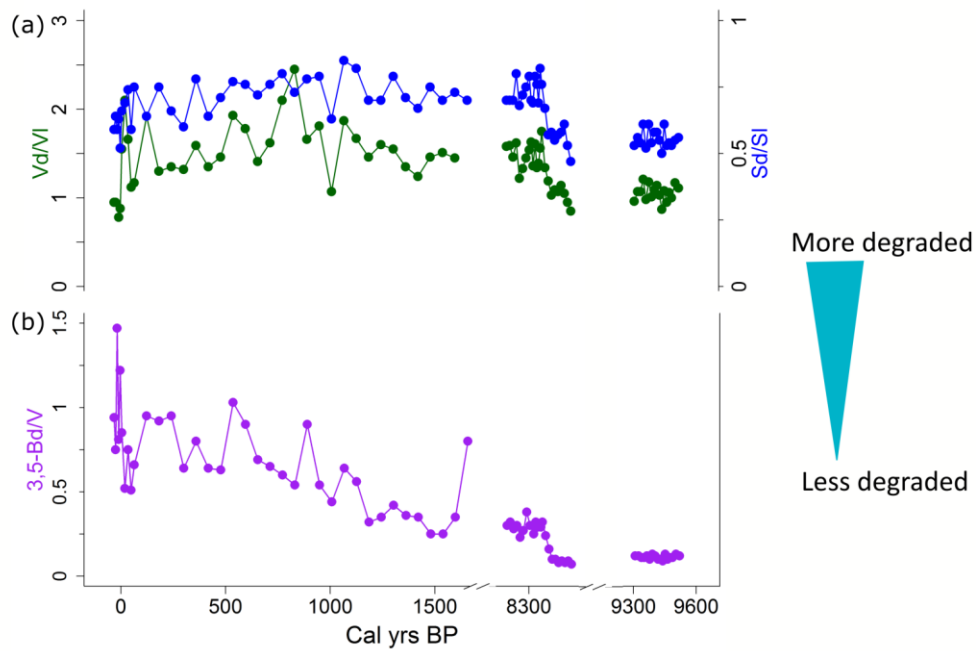
Field Code Changed

Formatted: Font: Bold

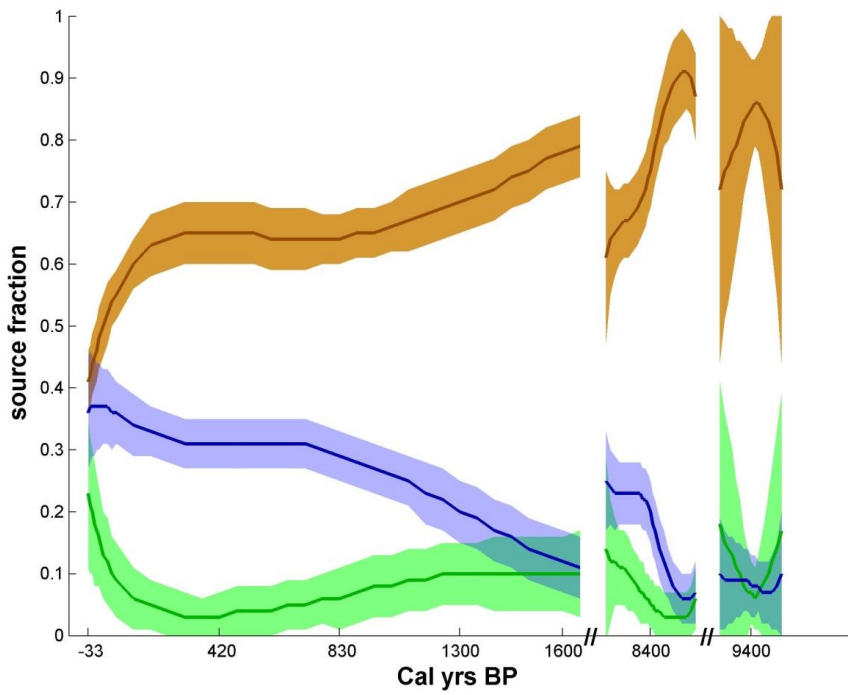
790 | are colored red. The blue shading indicates the modelled 2σ probability intervals for the entire depth range of the
791 | core and the tiny black curves 2σ for the individual measurements.
792



794 **Figure 3. Organic matter composition of the sediment core GC58. The x-axis has breaks due to gaps in the sediment**
795 **chronology. (a) Organic carbon fluxes ($\text{g m}^{-2} \text{yr}^{-1}$) were high at the bottom of the core. The high fluxes at the top of**
796 **the core are likely related to the merging of two dating system (^{210}Pb and ^{14}C , see Sect. 3.2). The sea level rose rapidly**
797 **in the early Holocene (Lambeck et al., 2014). (b) Both lignin and cutin fluxes ($\text{mg m}^{-2} \text{yr}^{-1}$) decrease toward the core**
798 **top. High fluxes at the top of the core are influenced by the OC fluxes and likely do not show an actual increase in the**
799 **fluxes of lignin and cutin (see Sect. 3.2). (c) Low molecular weight fatty acids (LMW-FA) show an influence of marine**
800 **organic matter at the top of the core. (d) The $\delta^{13}\text{C}$ (‰) values illustrate a gradual shift from terrestrial dominated to**
801 **more marine dominated input of organic matter towards the core top. The $\Delta^{14}\text{C}$ (‰) values (corrected for the time**
802 **between the deposition and the measurement) show that the bulk organic carbon is older at the bottom of the core**
803 **than at the core top. The drop in the $\Delta^{14}\text{C}$ values $\sim 1,700$ cal yrs BP is likely an artefact caused by the age model used**
804 **to correct for the $\Delta^{14}\text{C}$ values.**
805

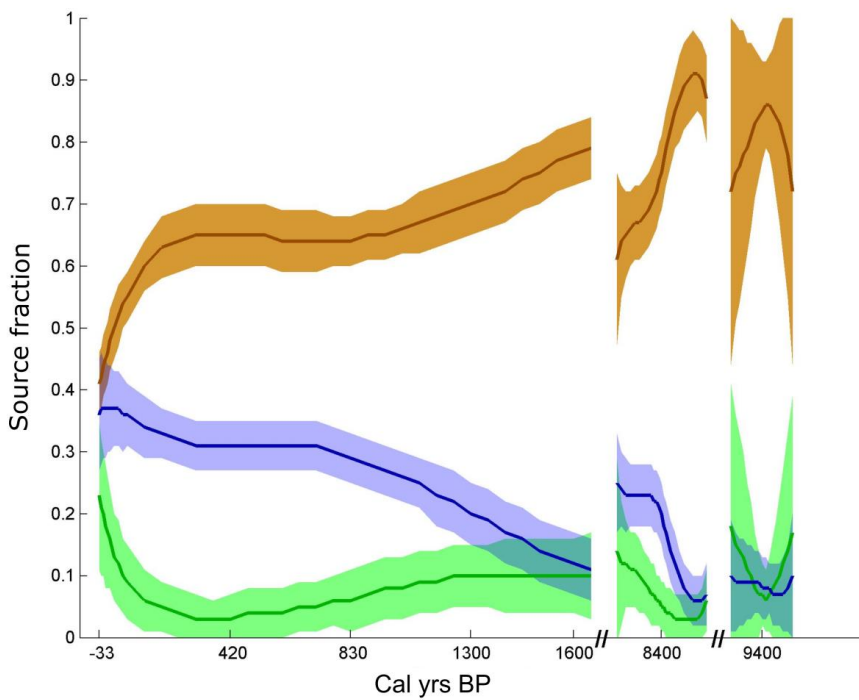


806
807 **Figure 4. Degradation proxies for terrestrial organic carbon in the sediment core GC58. The x-axis has breaks due to**
808 **gaps in the sediment chronology. (a) Syringyl acid to syringaldehyde (Sd/SI) and vanillic acid to vanillin (Vd/Vl)**
809 **ratios are a lignin-phenol based degradation proxy. (b) Also the ratio of 3,5-dihydrobenzoic acid to vanillyl phenols**
810 **(3,5-Bd/V) provides information on degradation of terrestrial organic carbon. Higher values imply more degraded**
811 **material for all the ratios as illustrated with the turquoise arrow. The 3,5-Bd/V values suggest a gradual increase in**
812 **degradation from the bottom of the core to the top.**
813



Formatted: Font: (Default) Times New Roman

814



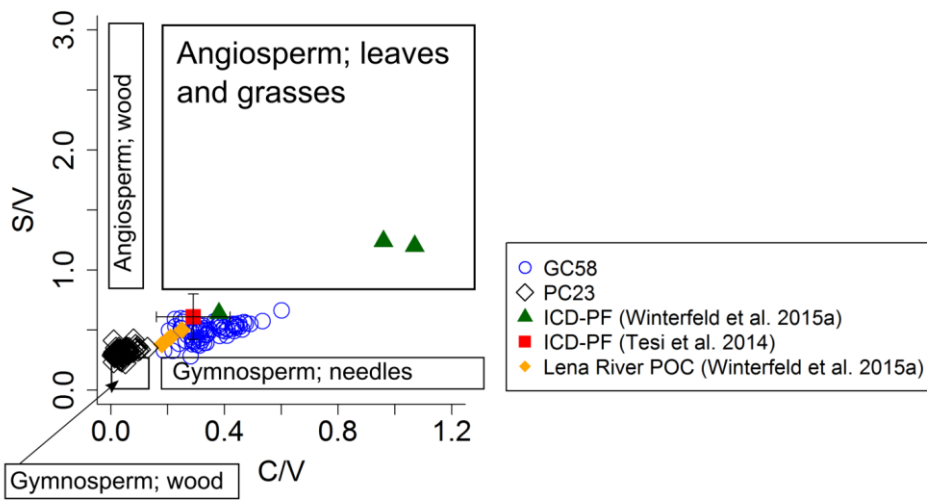
Formatted: Font: (Default) Times New Roman

815

816 **Figure 54.** Dual-carbon isotope ($\delta^{13}\text{C}$, $\Delta^{14}\text{C}$) based source apportionment of organic carbon (OC) illustrates fractions
 817 (%; mean \pm SD) of old Pleistocene permafrost (ICD-PF) in brown, thaw of active-layer permafrost (topsoil-PF) in

818 green and primary production (marine OC) in blue of the sediment core GC58. The ICD-PF is the dominant fraction
819 throughout the core.
820

821



Formatted: Font: (Default) Times New Roman

822

823

824

825

826

827

828

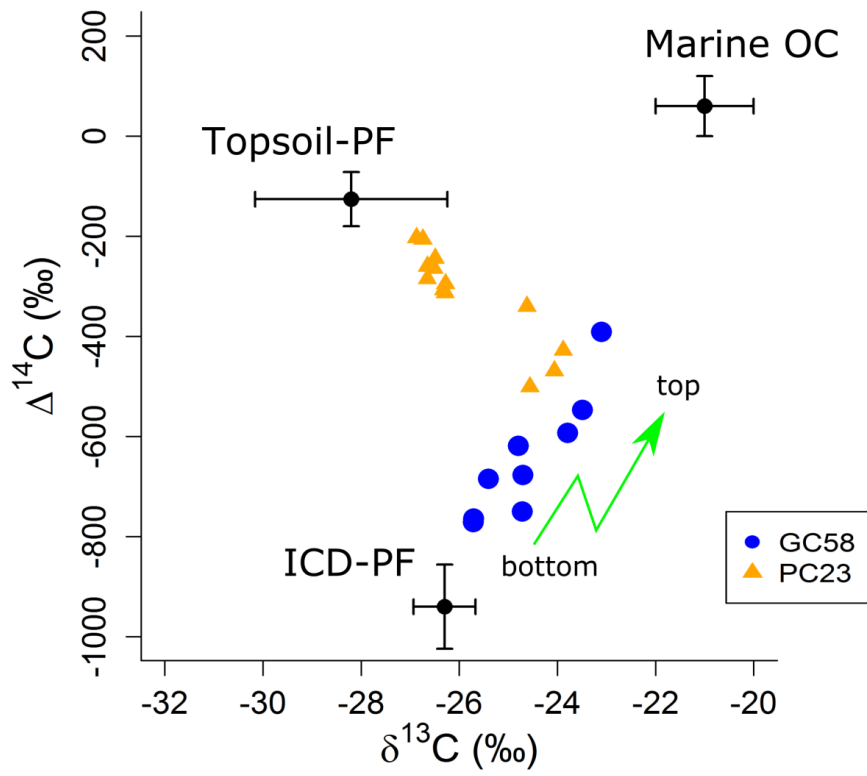
829

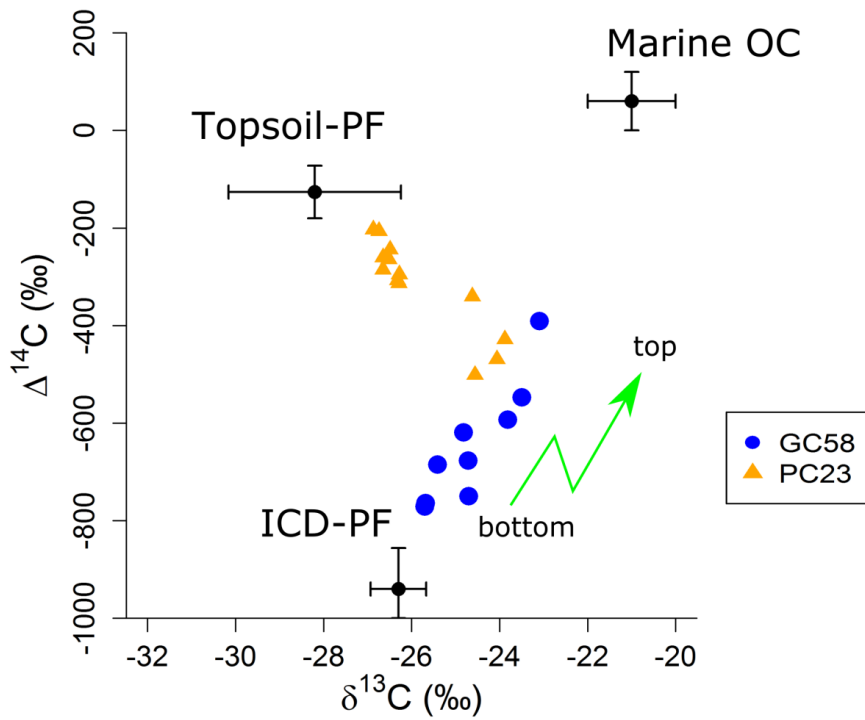
830

831

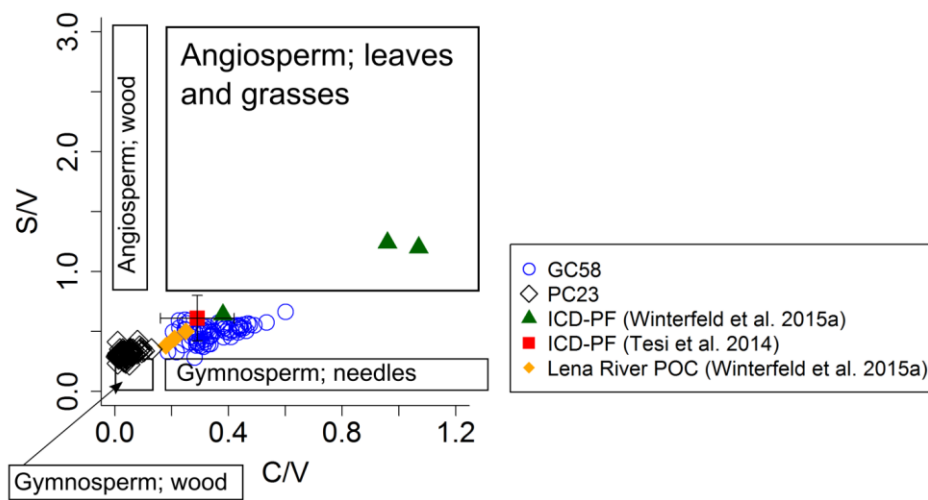
Figure 6. Lignin composition of the sediment core GC58 (black circles). The ratio between cinnamyl and vanillyl phenols (C/V) is used as a proxy to distinguish between soft and woody plant tissues. The ratio of syringyl to vanillyl phenols (S/V) indicates the difference between gymnosperm and angiosperm plants. The boxes indicate typical values for S/V and C/V ratios characterising different plant material (ranges from Coñi and Montgomery, 2000). Measured S/V and C/V ratios for Ice-Complex Deposit permafrost (ICD-PF) are shown with green triangles (Winterfeld et al., 2015a) and with an orange square (±standard deviation) (Tesi et al., 2014). Measured S/V and C/V ratios for topsoil-PF (Lena River POC) are illustrated with orange diamonds (Winterfeld et al., 2015a). Also shown the lignin composition of the sediment core PC23 (blue diamonds) from the Laptev Sea.

Field Code Changed





833
834 Figure 57. Dual-carbon isotope ($\delta^{13}\text{C}$, $\Delta^{14}\text{C}$) composition of the sediment cores GC58 (this study) and PC23 (Tesi et
835 al., 2016a). Topsoil-PF refers to organic matter from the active-layer of permafrost, ICD-PF to relict Pleistocene Ice
836 Complex Deposit permafrost (Yedoma) and marine OC to organic matter from primary production. The end-
837 member values for different sources are taken from the literature (Bröder et al., 2016b; Tesi et al., 2016a). The end-
838 member values for different sources are taken from a dataset compiled by Vonk et al., (2012) and a study by (Smith
839 et al., 2002). The green arrow points to the direction from the bottom to the top of the core (GC58).
840

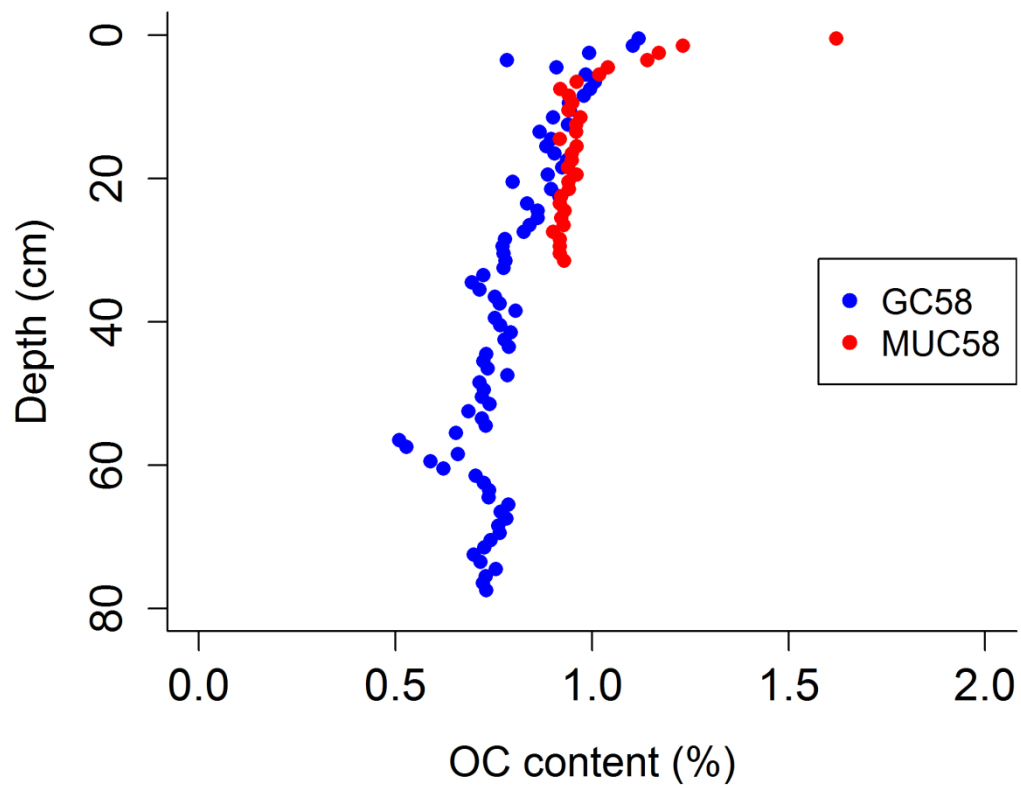


841
 842 | Figure 6. Lignin composition of the sediment core GC58 (~~black-blue~~ circles). The ratio between cinnamyl and vanillyl
 843 | phenols (C/V) is used as a proxy to distinguish between soft and woody plant tissues. The ratio of syringyl to vanillyl
 844 | phenols (S/V) indicates the difference between gymnosperm and angiosperm plants. The boxes indicate typical values
 845 | for S/V and C/V ratios characterising different plant material (ranges from Goñi and Montgomery, 2000). Measured
 846 | S/V and C/V ratios for Ice Complex Deposit permafrost (ICD-PF) are shown with green triangles (Winterfeld et al.,
 847 | 2015) and with an ~~red orange~~-square (\pm standard deviation) (Tesi et al., 2014). Measured S/V and C/V ratios for
 848 | topsoil-PF (Lena River POC) are illustrated with orange diamonds (Winterfeld et al., 2015). Also shown the lignin
 849 | composition of the sediment core PC23 (~~blue-black~~ diamonds) from the Laptev Sea ([study by Tesi et al., 2016a](#)).
 850

1 **Supplementary information**

2

3 **Tables and figures**



4

5 **Figure S1. Comparison between the organic carbon (OC) content (%) of the sediment cores GC58 and**
6 **MUC58. Based on the comparison, we deduced that the top 3cm of GC58 were lost during sampling.**

7 **Table S1. Total organic carbon (TOC) content, stable carbon isotopes ($\delta^{13}\text{C}$) and calibrated radiocarbon**
 8 **isotopes of bulk carbon (cal $\Delta^{14}\text{C}$) in the sediment core GC58 that were used for source apportionment**
 9 **calculations.**

Corrected depth* (cm)	TOC (%)	$\delta^{13}\text{C}$ (‰)	Cal $\Delta^{14}\text{C}$
3.5	1.12	-23.23	-400.17
4.5	1.10	-23.07	
5.5	0.99	-23.25	
6.5	0.78	-23.10	
7.5	0.91	-23.16	
8.5	0.99	-23.32	
9.5	1.01	-23.12	
10.5	1.00	-23.42	
11.5	0.98	-23.48	
12.5	0.94	-23.39	
13.5	0.94	-23.19	-568.02
14.5	0.90	-23.32	
15.5	0.94	-23.38	
16.5	0.87	-23.49	
17.5	0.90	-23.61	
18.5	0.88	-23.56	
19.5	0.91	-23.61	
20.5	0.94	-23.44	
21.5	0.93	-23.62	
22.5	0.89	-23.57	
23.5	0.80	-23.50	-604.39
24.5	0.90	-23.56	
25.5	0.92	-23.59	
26.5	0.84	-23.76	
27.5	0.86	-23.57	
28.5	0.86	-23.88	
29.5	0.84	-23.61	
30.5	0.83	-24.33	
31.5	0.78	-24.08	
32.5	0.77	-24.22	
33.5	0.78	-23.89	-679.07
34.5	0.78	-24.14	
35.5	0.78	-24.24	
36.5	0.72	-24.73	
37.5	0.70	-24.54	
38.5	0.71	-24.63	-747.85
39.5	0.75	-24.37	
40.5	0.77	-24.82	
41.5	0.81	-24.75	
42.5	0.75	-24.95	
43.5	0.77	-25.07	-586.93
44.5	0.79	-24.91	

45.5	0.78	-24.91	
46.5	0.79	-24.93	
47.5	0.73	-24.86	-607.58
48.5	0.72	-24.93	
49.5	0.74	-25.01	
50.5	0.79	-24.85	
51.5	0.71	-25.08	
52.5	0.73	-25.05	
53.5	0.72	-25.11	-680.66
54.5	0.74	-24.85	
55.5	0.69	-25.34	
56.5	0.72	-25.44	
57.5	0.73	-25.51	
58.5	0.65	-25.66	
59.5	0.51	-25.65	
60.5	0.53	-25.68	
61.5	0.66	-25.55	
62.5	0.59	-25.65	
63.5	0.62	-25.74	-771.72
64.5	0.71	-25.59	
65.5	0.73	-25.68	
66.5	0.74	-25.66	
67.5	0.74	-25.66	
68.5	0.79	-25.53	
69.5	0.77	-25.51	
70.5	0.78	-25.63	
71.5	0.76	-25.60	
72.5	0.77	-25.59	
73.5	0.74	-25.66	-764.43
74.5	0.73	-25.60	
75.5	0.70	-25.59	
76.5	0.72	-25.70	
77.5	0.76	-25.65	
78.5	0.73	-25.84	
79.5	0.72	-25.75	
80.5	0.73	-25.58	

10 *Corrected depth is the original depth + 3 cm to account for core top loss during sampling (Sect. 2.4).

11

12 **Table S2. The amount of excess ^{210}Pb (Bq g^{-1}) and natural logarithm (ln) of excess ^{210}Pb in the sediment**
 13 **core MUC58 and age chronology (CRC and CIC models) presented as age (yr) and resulting year of**
 14 **deposition. The CRC model assumes a constant rate of supply of ^{210}Pb fallout, as the CIC assumes the**
 15 **initial concentration of ^{210}Pb to be constant (Appleby & Oldfield, 1977). The highest ^{137}Cs peak was in 4.5**
 16 **cm depth.**

Depth (cm)	Excess ^{210}Pb (Bq g^{-1})	Ln of excess ^{210}Pb	Age (yr) with CRC model	Resulting year with CRC model	Age (yr) with CIC model	Resulting year with CIC model	OC flux ($\text{g m}^{-2} \text{yr}^{-1}$)
0.5	0.062	-2.78	0	2014	4	2010	6.1
1.5	0.061	-2.79	6	2008	12	2002	4.6
2.5	0.054	-2.92	14	2000	20	1994	4.4
3.5	0.049	-3.02	23	1991	28	1986	4.3
4.5	0.024	-3.73	35	1979	36	1978	3.9
5.5	0.016	-4.11	42	1972	44	1970	3.8
6.5	0.014	-4.24	49	1965	52	1962	3.6
7.5	0.021	-3.86	55	1959	60	1954	3.4
8.5	0.016	-4.145	69	1945	68	1946	3.5
9.5	0.006	-5.16	85	1929	75	1939	3.6
10.5	0.001	-6.67	94	1920	83	1931	3.5
11.5	0.012	-4.41	96	1918	91	1923	3.6
12.5	0.005	-5.25	134	1880	99	1915	0.4

17 **Table S3. Biomarker data for the sediment core GC58. S = syringyl phenols, V = vanillyl phenols, C = cinnamyl phenols, 3,5-Bd = 3,5-Dihydroxybenzoic acid, Cut =**
 18 **sum of all cutin acids, FA = sum of all CuO oxidation-derived fatty acids, Lig = sum of all lignin phenols, Sd = syringic acid, Sl = syringaldehyde, Vd = vanillic acid,**
 19 **VI = vanillin (see Supplementary Table S4 for full list of compounds and their origin).**

20

Corrected depth*	S	V	C	3,5-Bd	Cut	FA	Lig	S/V	C/V	Sd/Sl	Vd/VI	3,5-Bd/V
cm	mg g OC ⁻¹											
3.5	0.05	0.13	0.04	0.1225	0.27	5.35	0.2244	0.42	0.31	0.59	0.95	0.94
4.5	0.08	0.12	0.07	0.0898	0.30	3.17	0.2700	0.66	0.60	0.64	0.95	0.75
5.5	0.07	0.08	0.03	0.1148	0.24	2.55	0.1770	0.90	0.37	0.59	0.00	1.47
6.5	0.07	0.12	0.03	0.1008	0.30	2.55	0.2318	0.59	0.26	0.63	0.78	0.81
7.5	0.07	0.12	0.03	0.1486	0.30	2.06	0.2222	0.59	0.23	0.52	0.88	1.22
8.5	0.05	0.12	0.03	0.1055	0.27	1.38	0.2017	0.39	0.24	0.66	1.55	0.85
9.5	0.04	0.13	0.04	0.0696	0.27	1.26	0.2071	0.28	0.28	0.69	2.10	0.52
10.5	0.05	0.14	0.04	0.1043	0.28	1.41	0.2349	0.37	0.31	0.74	1.66	0.75
11.5	0.10	0.21	0.09	0.1083	0.34	1.31	0.4051	0.49	0.43	0.59	1.12	0.51
12.5	0.05	0.15	0.03	0.0978	0.34	1.53	0.2304	0.33	0.22	0.75	1.17	0.66
13.5	0.04	0.09	0.03	0.0866	0.29	1.35	0.1603	0.43	0.32	0.64	1.92	0.95
14.5	0.05	0.14	0.05	0.1276	0.35	1.43	0.2386	0.39	0.33	0.75	1.30	0.92
15.5	0.05	0.10	0.03	0.0917	0.27	1.12	0.1763	0.48	0.35	0.66	1.35	0.95
16.5	0.05	0.16	0.03	0.1005	0.28	1.40	0.2383	0.33	0.19	0.60	1.32	0.64
17.5	0.05	0.14	0.05	0.1092	0.35	1.43	0.2356	0.39	0.34	0.78	1.59	0.80
18.5	0.05	0.12	0.04	0.0741	0.33	1.32	0.2125	0.45	0.38	0.64	1.35	0.64
19.5	0.05	0.13	0.04	0.0831	0.30	1.14	0.2190	0.38	0.29	0.71	1.46	0.63
20.5	0.05	0.09	0.02	0.0969	0.30	1.20	0.1668	0.52	0.25	0.77	1.93	1.03
21.5	0.05	0.10	0.05	0.0928	0.34	1.28	0.2033	0.50	0.46	0.76	1.78	0.90
22.5	0.06	0.16	0.05	0.1101	0.37	1.56	0.2716	0.40	0.29	0.72	1.41	0.69
23.5	0.07	0.17	0.05	0.1140	0.38	1.76	0.2973	0.41	0.29	0.76	1.62	0.65
24.5	0.06	0.15	0.05	0.0931	0.33	1.19	0.2595	0.38	0.30	0.80	2.10	0.60
25.5	0.06	0.15	0.04	0.0830	0.37	1.16	0.2581	0.41	0.26	0.73	2.45	0.54
26.7	0.07	0.15	0.05	0.1321	0.41	1.31	0.2686	0.49	0.33	0.78	1.66	0.90
27.5	0.06	0.15	0.05	0.0829	0.31	0.95	0.2650	0.41	0.32	0.79	1.81	0.54

28.5	0.08	0.18	0.05	0.0812	0.16	1.01	0.3152	0.46	0.27	0.63	1.07	0.44
29.5	0.08	0.19	0.06	0.1247	0.40	1.28	0.3308	0.41	0.29	0.85	1.87	0.64
30.5	0.12	0.26	0.09	0.1479	0.52	1.22	0.4713	0.46	0.34	0.82	1.67	0.56
31.5	0.14	0.29	0.11	0.0942	0.60	1.31	0.5506	0.50	0.39	0.70	1.46	0.32
32.5	0.15	0.31	0.13	0.1060	0.55	1.19	0.5871	0.51	0.41	0.70	1.60	0.35
33.5	0.15	0.33	0.13	0.1388	0.54	1.29	0.6118	0.45	0.41	0.79	1.55	0.42
34.5	0.16	0.35	0.10	0.1264	0.57	1.44	0.6116	0.44	0.28	0.71	1.35	0.36
35.5	0.23	0.46	0.13	0.1608	0.70	1.49	0.8146	0.49	0.29	0.67	1.24	0.35
36.5	0.22	0.44	0.09	0.1100	0.49	0.90	0.7432	0.50	0.20	0.75	1.46	0.25
37.5	0.21	0.39	0.09	0.0997	0.66	0.79	0.6890	0.53	0.23	0.70	1.51	0.25
38.5	0.28	0.55	0.17	0.1922	0.82	1.28	1.0034	0.50	0.32	0.73	1.45	0.35
39.5	0.25	0.33	0.16	0.2636	0.91	1.27	0.7434	0.77	0.49	0.70	0.00	0.80
40.5	0.25	0.48	0.17	0.1434	0.71	1.20	0.8986	0.51	0.35	0.70	1.58	0.30
41.5	0.24	0.47	0.18	0.1524	0.82	0.97	0.8947	0.50	0.39	0.70	1.59	0.32
42.5	0.28	0.53	0.17	0.1501	0.87	0.95	0.9828	0.52	0.32	0.70	1.46	0.28
43.5	0.27	0.55	0.23	0.1655	0.90	1.04	1.0439	0.49	0.42	0.80	1.62	0.30
44.5	0.24	0.59	0.15	0.1357	0.52	0.83	0.9758	0.40	0.24	0.68	1.22	0.23
45.5	0.31	0.57	0.21	0.1540	1.02	1.00	1.0923	0.53	0.37	0.72	1.33	0.27
46.5	0.28	0.61	0.17	0.2329	0.86	1.17	1.0583	0.46	0.27	0.75	1.45	0.38
47.5	0.28	0.60	0.20	0.1796	0.89	1.07	1.0789	0.46	0.34	0.79	1.54	0.30
48.5	0.33	0.63	0.24	0.1880	1.03	1.11	1.1976	0.52	0.38	0.70	1.63	0.30
49.5	0.26	0.53	0.16	0.1326	0.84	0.87	0.9443	0.49	0.31	0.69	1.36	0.25
50.5	0.27	0.53	0.17	0.1713	0.81	0.91	0.9745	0.51	0.33	0.79	1.61	0.32
51.5	0.33	0.68	0.20	0.1953	0.95	1.32	1.2145	0.49	0.30	0.76	1.34	0.29
52.5	0.40	0.71	0.18	0.2140	0.94	1.05	1.2953	0.57	0.25	0.69	1.39	0.30
53.5	0.29	0.60	0.24	0.1764	0.92	0.93	1.1337	0.49	0.40	0.82	1.56	0.29
54.5	0.31	0.60	0.15	0.1932	0.97	1.01	1.0656	0.51	0.25	0.76	1.75	0.32
55.5	0.53	0.99	0.32	0.2323	1.15	0.96	1.8391	0.53	0.33	0.67	1.34	0.24
56.5	0.61	1.27	0.36	0.1990	0.72	0.88	2.2406	0.48	0.29	0.57	1.19	0.16
57.5	1.10	2.16	0.93	0.2084	1.58	0.86	4.1854	0.51	0.43	0.58	1.03	0.10
58.5	1.23	2.14	0.79	0.2092	1.69	0.87	4.1617	0.57	0.37	0.55	1.09	0.10
59.5	1.21	2.33	0.93	0.1797	1.18	1.38	4.4684	0.52	0.40	0.57	1.07	0.08

60.5	1.23	2.18	1.02	0.2039	1.73	1.04	4.4373	0.57	0.47	0.58	1.14	0.09
61.5	1.35	2.77	0.79	0.2295	1.64	1.04	4.9075	0.49	0.28	0.61	1.05	0.08
62.5	1.51	2.74	1.18	0.2587	1.90	1.27	5.4277	0.55	0.43	0.53	0.95	0.09
63.5	1.80	3.20	1.22	0.2237	1.74	0.97	6.2276	0.56	0.38	0.47	0.85	0.07
64.5	1.27	2.40	0.93	0.2790	1.81	1.26	4.6095	0.53	0.39	0.53	0.96	0.12
65.5	1.15	2.07	0.94	0.2470	1.79	0.92	4.1586	0.55	0.45	0.56	1.07	0.12
66.5	1.27	2.38	0.74	0.2618	1.79	1.02	4.3928	0.53	0.31	0.54	1.07	0.11
67.5	1.00	1.79	0.85	0.1983	1.57	0.71	3.6389	0.56	0.48	0.61	1.21	0.11
68.5	1.19	2.18	0.84	0.2506	1.76	0.91	4.1993	0.55	0.38	0.52	0.98	0.12
69.5	0.85	1.71	0.53	0.1673	0.84	0.68	3.0966	0.50	0.31	0.61	1.18	0.10
70.5	1.31	2.46	0.92	0.3261	1.78	0.97	4.7013	0.53	0.38	0.54	1.01	0.13
71.5	1.25	2.32	1.02	0.2840	1.73	1.01	4.5828	0.54	0.44	0.58	1.09	0.12
72.5	1.20	2.19	0.96	0.2213	1.81	0.93	4.3449	0.55	0.44	0.58	1.14	0.10
73.5	1.04	2.07	0.72	0.2024	1.13	0.80	3.8276	0.50	0.35	0.55	1.03	0.10
74.5	1.41	2.68	1.22	0.2547	1.97	1.01	5.3135	0.53	0.45	0.50	0.87	0.09
75.5	1.39	2.62	1.16	0.3377	1.97	1.29	5.1729	0.53	0.44	0.61	1.08	0.13
76.5	1.30	2.48	1.09	0.2550	1.93	1.23	4.8662	0.52	0.44	0.53	0.95	0.10
77.5	1.14	2.00	1.07	0.2116	1.66	0.93	4.2050	0.57	0.53	0.54	1.06	0.11
78.5	1.25	2.30	1.02	0.2549	1.81	1.06	4.5619	0.54	0.44	0.53	1.00	0.11
79.5	1.23	2.15	1.02	0.2753	1.94	1.26	4.4096	0.57	0.48	0.55	1.17	0.13
80.5	1.22	2.22	1.09	0.2613	1.99	1.02	4.5331	0.55	0.49	0.56	1.11	0.12

21 * Corrected depth is the original depth + 3 cm to account for core top loss during sampling (Sect. 2.4)

22 **Table S4. CuO-derived compounds (adapted from Tesi et al. 2014 and references therein). MS means that the**
 23 **compound has multiple sources but is relatively abundant in the source mentioned.**

24

Group name	Name	Abbreviation	Source
Lignin phenols	Vanillyl phenols	V	Cell walls of angiosperm/gymnosperm vascular plants
	Vanillin	Vl	
	Acetovanillone	Vn	
	Vanillic acid	Vd	
	Syringyl phenols	S	Cell walls of angiosperm vascular plants
	Syringaldehyde	Sl	
	Acetosyringone	Sn	
	Syringic acid	Sd	
	Cinnamyl phenols	C	Non-woody vascular plant tissues
	<i>p</i> -Coumaric acid	pCd	
Ferulic acid	Fd		
Cutin products	Hydroxyhexadecanoic acid	ω -C16	Leaves; blades and needles of vascular plants
	Hexadecan-1,16-dioic acid	C16DA	
	18-Hydroxyoctadec-9-enoic acid	ω -C18:1	
	7 or 8-Dihydroxy C16 α , ω -dioic acids	α -OH, C16DA	
	8, 9 or 10-Dihydroxy C16 acids	α , ω -OH C16	
Hydroxy benzene products	Benzoic acid	Bd	Phytoplankton and soil (MS)
	<i>m</i> -Hydroxybenzoic acid	<i>m</i> -Bd	Abundant in soil
	3,5-Dihydroxybenzoic acid	3,5-Bd	
Fatty acids	Octanoic acid	C8FA	Phytoplankton (MS)
	Decanoic acid	C10FA	Bacteria
	Dodecanoic acid	C12FA	Bacteria (MS)
	Tetradecanoic acid	C14FA	Phytoplankton (MS)
	Hexadecanoic acids	C16FA:1, C16FA	Phytoplankton and soil (also bacteria for C16FA:1) (MS)
	Octadecanoic acids	C18FA:1, C18FA	Phytoplankton and soil (also bacteria for C18FA:1) (MS)

25

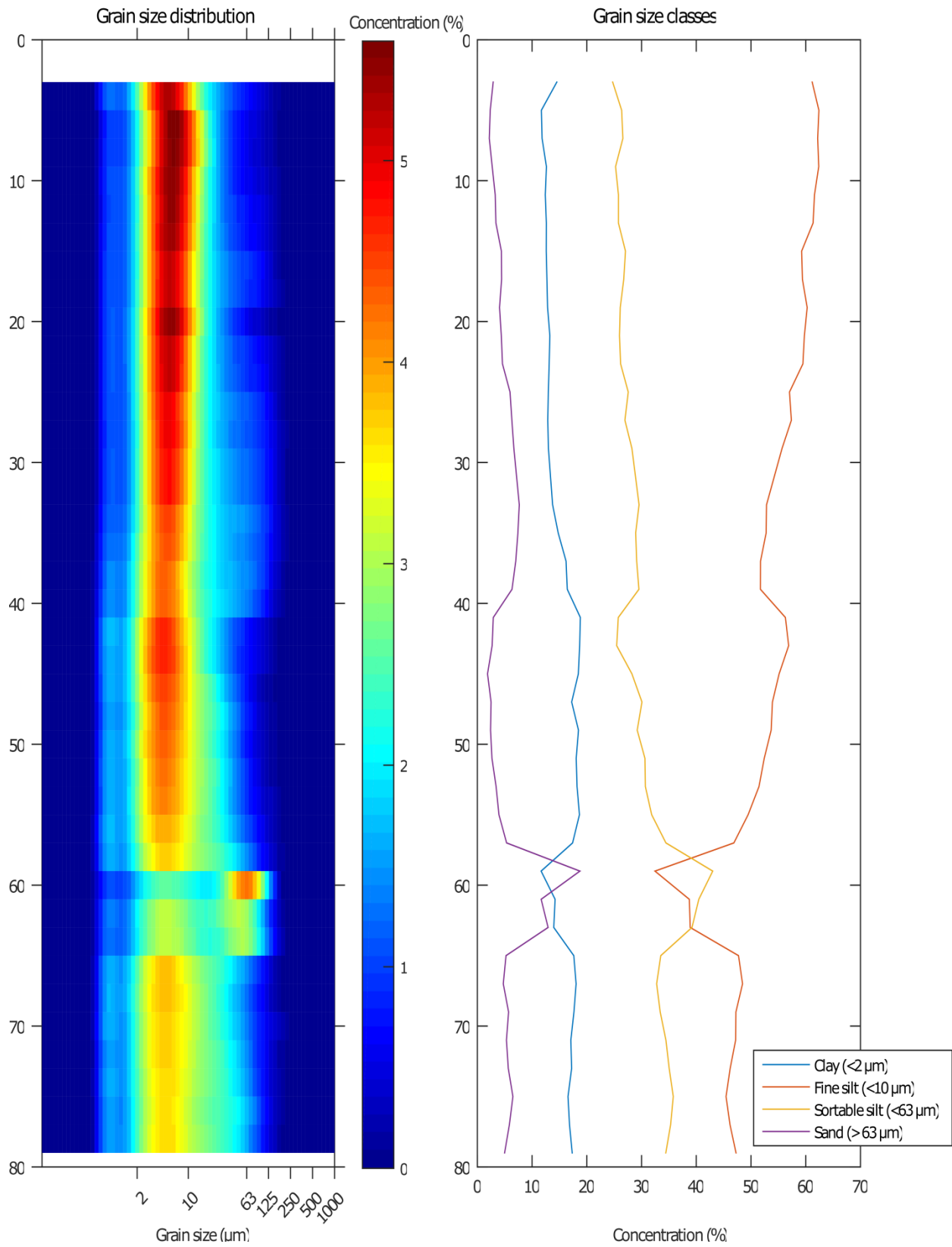
26 **Table S5. Source apportionment data from the Monte Carlo Mixing Model based on carbon isotopes ($\Delta^{14}\text{C}$, $\delta^{13}\text{C}$) as fractions (mean and median, %) for the**
 27 **sediment core GC58, including 5th (q05) and 9th (q95) percentiles and standard deviation (sd). Topsoil-PF (topsoil permafrost) refers to thaw of the active-layer**
 28 **permafrost, ICD-PF (Ice Complex Deposit permafrost) represents old Pleistocene material from coastal erosion and marine OC (organic carbon) to primary**
 29 **production of phytoplankton.**

Corrected depth (cm)	ICD-PF					Topsoil-PF					Marine OC				
	mean	median	sd	q05	q95	mean	median	sd	q05	q95	mean	median	sd	q05	q95
3.5	0.407	0.406	0.050	0.328	0.489	0.230	0.210	0.120	0.066	0.450	0.363	0.377	0.094	0.196	0.498
4.5	0.422	0.421	0.048	0.347	0.503	0.212	0.194	0.111	0.062	0.416	0.366	0.377	0.088	0.207	0.492
5.5	0.437	0.435	0.047	0.363	0.516	0.196	0.179	0.103	0.057	0.386	0.367	0.377	0.083	0.217	0.487
6.5	0.451	0.449	0.046	0.379	0.529	0.181	0.165	0.095	0.053	0.358	0.368	0.378	0.079	0.225	0.481
7.5	0.464	0.462	0.046	0.394	0.542	0.167	0.152	0.089	0.049	0.334	0.369	0.377	0.075	0.233	0.477
8.5	0.476	0.474	0.046	0.407	0.555	0.155	0.141	0.084	0.045	0.312	0.369	0.376	0.071	0.240	0.472
9.5	0.499	0.497	0.045	0.431	0.578	0.133	0.120	0.074	0.038	0.273	0.368	0.374	0.065	0.251	0.462
10.5	0.519	0.517	0.045	0.452	0.597	0.116	0.104	0.067	0.031	0.241	0.365	0.370	0.059	0.258	0.453
11.5	0.536	0.534	0.045	0.470	0.615	0.101	0.090	0.061	0.025	0.216	0.362	0.366	0.055	0.264	0.444
12.5	0.552	0.550	0.045	0.487	0.630	0.090	0.078	0.057	0.021	0.195	0.358	0.362	0.052	0.267	0.436
13.5	0.597	0.595	0.044	0.534	0.674	0.060	0.050	0.045	0.010	0.142	0.342	0.346	0.045	0.265	0.412
14.5	0.625	0.623	0.045	0.561	0.702	0.046	0.036	0.040	0.006	0.115	0.329	0.331	0.044	0.255	0.397
15.5	0.642	0.641	0.046	0.575	0.719	0.038	0.029	0.037	0.004	0.101	0.319	0.321	0.044	0.246	0.388
16.5	0.651	0.650	0.047	0.583	0.728	0.035	0.026	0.035	0.003	0.094	0.314	0.315	0.044	0.241	0.384
17.5	0.654	0.653	0.047	0.586	0.732	0.034	0.025	0.035	0.003	0.092	0.312	0.313	0.044	0.238	0.382
18.5	0.653	0.652	0.047	0.587	0.731	0.035	0.025	0.035	0.003	0.093	0.312	0.314	0.044	0.238	0.381
19.5	0.650	0.648	0.046	0.586	0.728	0.037	0.027	0.036	0.003	0.098	0.313	0.315	0.044	0.239	0.381
20.5	0.645	0.643	0.046	0.583	0.724	0.040	0.030	0.037	0.004	0.105	0.314	0.317	0.044	0.239	0.382
21.5	0.641	0.638	0.046	0.579	0.720	0.044	0.034	0.039	0.005	0.114	0.314	0.317	0.044	0.239	0.382
22.5	0.639	0.635	0.045	0.578	0.718	0.049	0.039	0.041	0.005	0.123	0.312	0.315	0.044	0.236	0.380
23.5	0.638	0.634	0.045	0.577	0.717	0.054	0.044	0.043	0.006	0.131	0.308	0.311	0.044	0.232	0.376
24.5	0.639	0.635	0.045	0.578	0.719	0.059	0.049	0.044	0.008	0.140	0.302	0.305	0.044	0.226	0.370
25.5	0.641	0.637	0.045	0.581	0.722	0.064	0.055	0.046	0.010	0.148	0.294	0.297	0.044	0.218	0.362
26.5	0.646	0.641	0.045	0.585	0.727	0.070	0.061	0.047	0.011	0.156	0.285	0.287	0.044	0.209	0.353
27.5	0.651	0.647	0.045	0.591	0.733	0.075	0.067	0.048	0.014	0.163	0.274	0.275	0.044	0.198	0.343

28.5	0.658	0.654	0.045	0.598	0.740	0.081	0.073	0.049	0.016	0.170	0.261	0.263	0.044	0.185	0.331
29.5	0.667	0.662	0.045	0.607	0.750	0.086	0.079	0.049	0.017	0.177	0.247	0.249	0.045	0.170	0.318
30.5	0.676	0.670	0.045	0.618	0.760	0.091	0.084	0.050	0.019	0.183	0.233	0.235	0.045	0.155	0.304
31.5	0.687	0.680	0.046	0.629	0.772	0.095	0.089	0.051	0.021	0.190	0.218	0.220	0.046	0.139	0.291
32.5	0.699	0.691	0.046	0.642	0.786	0.099	0.093	0.052	0.021	0.196	0.202	0.205	0.047	0.122	0.277
33.5	0.711	0.703	0.047	0.654	0.800	0.102	0.096	0.054	0.021	0.200	0.187	0.190	0.049	0.104	0.264
34.5	0.724	0.716	0.047	0.668	0.817	0.103	0.097	0.055	0.020	0.205	0.172	0.175	0.050	0.087	0.251
35.5	0.738	0.729	0.048	0.681	0.833	0.104	0.098	0.057	0.017	0.209	0.158	0.161	0.051	0.070	0.239
36.5	0.753	0.743	0.049	0.695	0.849	0.103	0.097	0.059	0.015	0.211	0.144	0.147	0.052	0.055	0.227
37.5	0.767	0.756	0.049	0.709	0.865	0.102	0.095	0.060	0.012	0.211	0.131	0.134	0.053	0.041	0.217
38.5	0.781	0.770	0.050	0.722	0.879	0.099	0.092	0.061	0.009	0.213	0.120	0.121	0.054	0.030	0.207
39.5	0.794	0.784	0.054	0.728	0.894	0.098	0.089	0.066	0.006	0.218	0.109	0.109	0.054	0.021	0.200
40.5	0.606	0.633	0.141	0.328	0.789	0.141	0.091	0.146	0.011	0.448	0.253	0.253	0.076	0.132	0.376
41.5	0.638	0.644	0.092	0.477	0.774	0.123	0.097	0.096	0.024	0.315	0.239	0.240	0.063	0.137	0.341
42.5	0.654	0.652	0.066	0.552	0.762	0.116	0.102	0.068	0.032	0.248	0.230	0.231	0.057	0.137	0.322
43.5	0.662	0.658	0.060	0.574	0.759	0.112	0.104	0.060	0.030	0.225	0.226	0.226	0.054	0.137	0.313
44.5	0.666	0.664	0.061	0.576	0.766	0.108	0.101	0.059	0.025	0.218	0.225	0.225	0.053	0.139	0.312
45.5	0.671	0.669	0.061	0.580	0.772	0.101	0.093	0.058	0.021	0.211	0.227	0.227	0.052	0.144	0.313
46.5	0.679	0.676	0.060	0.590	0.778	0.092	0.083	0.055	0.017	0.196	0.229	0.229	0.051	0.149	0.313
47.5	0.690	0.686	0.060	0.602	0.788	0.081	0.072	0.051	0.014	0.179	0.229	0.228	0.050	0.151	0.311
48.5	0.699	0.695	0.060	0.610	0.797	0.075	0.066	0.049	0.012	0.169	0.227	0.226	0.049	0.150	0.308
49.5	0.709	0.706	0.060	0.621	0.809	0.068	0.059	0.047	0.011	0.159	0.222	0.221	0.048	0.146	0.302
50.5	0.722	0.719	0.061	0.633	0.824	0.062	0.053	0.045	0.009	0.150	0.215	0.214	0.048	0.140	0.294
51.5	0.738	0.734	0.061	0.649	0.840	0.057	0.047	0.043	0.008	0.139	0.205	0.205	0.048	0.130	0.283
52.5	0.753	0.749	0.062	0.664	0.855	0.052	0.042	0.041	0.006	0.132	0.195	0.194	0.047	0.121	0.272
53.5	0.769	0.765	0.062	0.679	0.872	0.048	0.038	0.039	0.005	0.125	0.183	0.182	0.047	0.109	0.259
54.5	0.786	0.783	0.063	0.696	0.887	0.044	0.034	0.038	0.004	0.118	0.170	0.169	0.047	0.096	0.246
55.5	0.819	0.817	0.064	0.725	0.918	0.038	0.028	0.036	0.003	0.107	0.143	0.142	0.046	0.071	0.219
56.5	0.848	0.850	0.065	0.749	0.944	0.034	0.023	0.037	0.002	0.104	0.118	0.116	0.045	0.048	0.194
57.5	0.871	0.876	0.066	0.768	0.962	0.032	0.019	0.040	0.001	0.105	0.097	0.094	0.044	0.032	0.173
58.5	0.888	0.896	0.067	0.782	0.976	0.031	0.017	0.042	0.001	0.105	0.081	0.076	0.042	0.020	0.155
59.5	0.900	0.909	0.067	0.792	0.983	0.031	0.016	0.044	0.001	0.107	0.070	0.064	0.041	0.013	0.142

60.5	0.906	0.915	0.066	0.798	0.988	0.032	0.017	0.044	0.000	0.111	0.063	0.057	0.040	0.009	0.133
61.5	0.906	0.912	0.065	0.801	0.991	0.034	0.021	0.043	0.000	0.112	0.060	0.055	0.040	0.006	0.131
62.5	0.897	0.899	0.064	0.797	0.992	0.041	0.030	0.042	0.000	0.119	0.062	0.057	0.042	0.004	0.136
63.5	0.870	0.863	0.073	0.768	0.992	0.061	0.052	0.052	0.000	0.159	0.069	0.065	0.047	0.003	0.152
64.5	0.718	0.832	0.281	0.075	0.981	0.180	0.072	0.235	0.002	0.738	0.102	0.076	0.092	0.010	0.294
65.5	0.751	0.844	0.244	0.177	0.979	0.155	0.065	0.206	0.003	0.642	0.095	0.076	0.076	0.013	0.247
66.5	0.765	0.842	0.222	0.253	0.980	0.142	0.065	0.188	0.002	0.575	0.093	0.078	0.071	0.012	0.230
67.5	0.778	0.840	0.200	0.336	0.982	0.129	0.063	0.167	0.002	0.500	0.093	0.080	0.067	0.010	0.219
68.5	0.794	0.841	0.175	0.427	0.983	0.113	0.061	0.144	0.002	0.415	0.093	0.082	0.063	0.010	0.207
69.5	0.811	0.843	0.147	0.518	0.982	0.097	0.057	0.119	0.002	0.334	0.092	0.084	0.059	0.010	0.194
70.5	0.827	0.845	0.120	0.608	0.980	0.083	0.054	0.093	0.002	0.260	0.090	0.085	0.054	0.011	0.184
71.5	0.840	0.846	0.097	0.679	0.980	0.073	0.054	0.071	0.002	0.201	0.087	0.083	0.050	0.011	0.173
72.5	0.851	0.847	0.080	0.730	0.980	0.066	0.055	0.055	0.002	0.168	0.083	0.081	0.047	0.011	0.163
73.5	0.856	0.848	0.074	0.756	0.982	0.064	0.055	0.050	0.002	0.159	0.079	0.077	0.045	0.010	0.156
74.5	0.857	0.854	0.081	0.730	0.984	0.068	0.056	0.058	0.002	0.176	0.076	0.072	0.045	0.009	0.153
75.5	0.851	0.862	0.101	0.673	0.986	0.076	0.055	0.078	0.002	0.221	0.073	0.067	0.047	0.007	0.155
76.5	0.840	0.867	0.128	0.590	0.988	0.088	0.055	0.103	0.001	0.283	0.071	0.064	0.050	0.006	0.161
77.5	0.826	0.869	0.158	0.501	0.990	0.102	0.056	0.130	0.001	0.361	0.072	0.061	0.055	0.005	0.173
78.5	0.809	0.869	0.187	0.402	0.992	0.117	0.057	0.154	0.001	0.442	0.074	0.060	0.061	0.005	0.189
79.5	0.779	0.861	0.229	0.253	0.992	0.139	0.059	0.187	0.001	0.561	0.083	0.064	0.074	0.004	0.229
80.5	0.724	0.836	0.282	0.090	0.995	0.171	0.067	0.225	0.000	0.687	0.105	0.079	0.101	0.002	0.313

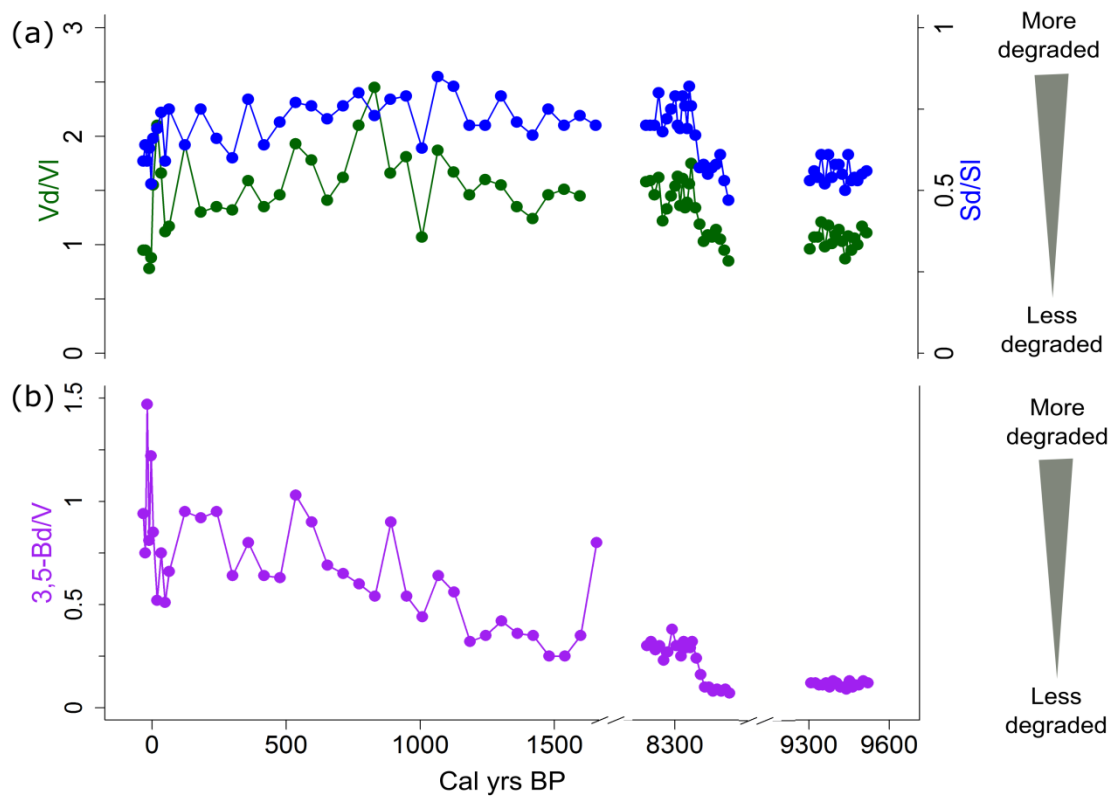
30 * Corrected depth is the original depth + 3 cm to account for core top loss during sampling (Sect 2.4)



31

32 **Figure S2. The grain size of the sediment core GC58. The GC58 core consists mainly of clay and silt with a**
 33 **fraction of sand around 60 cm of depth.**

34

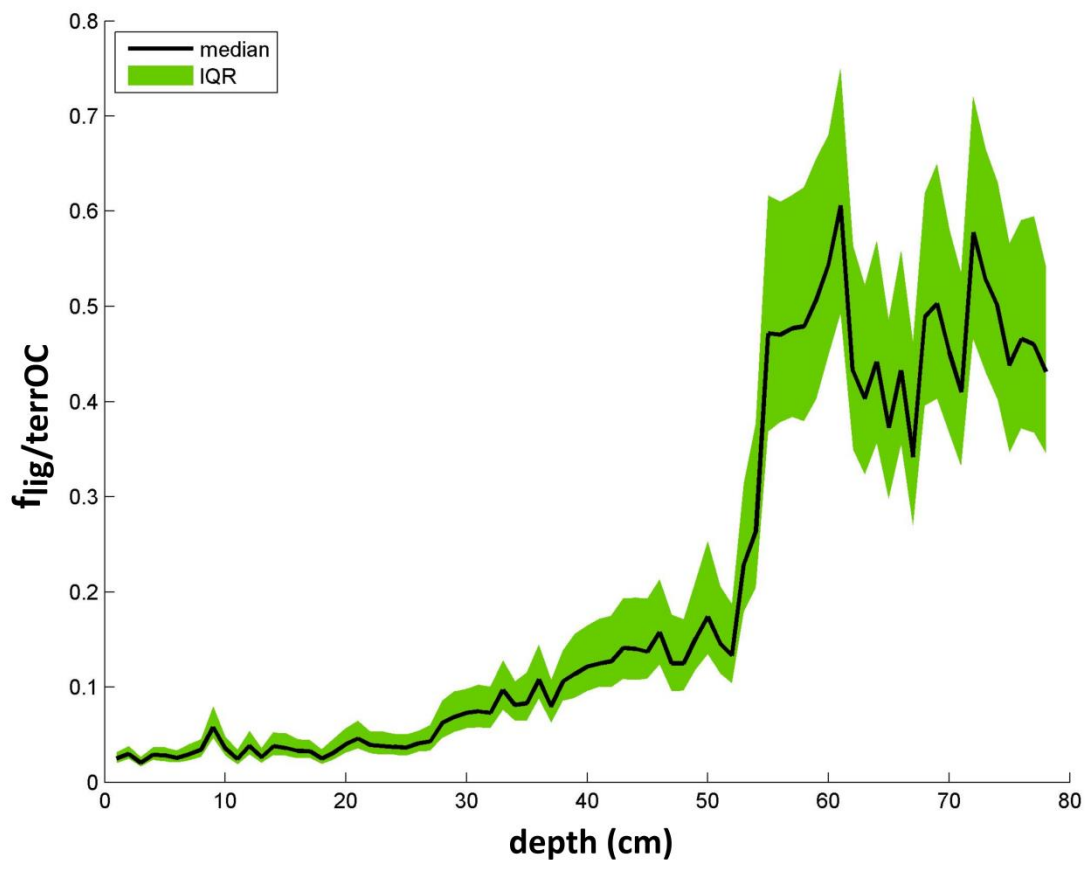


35

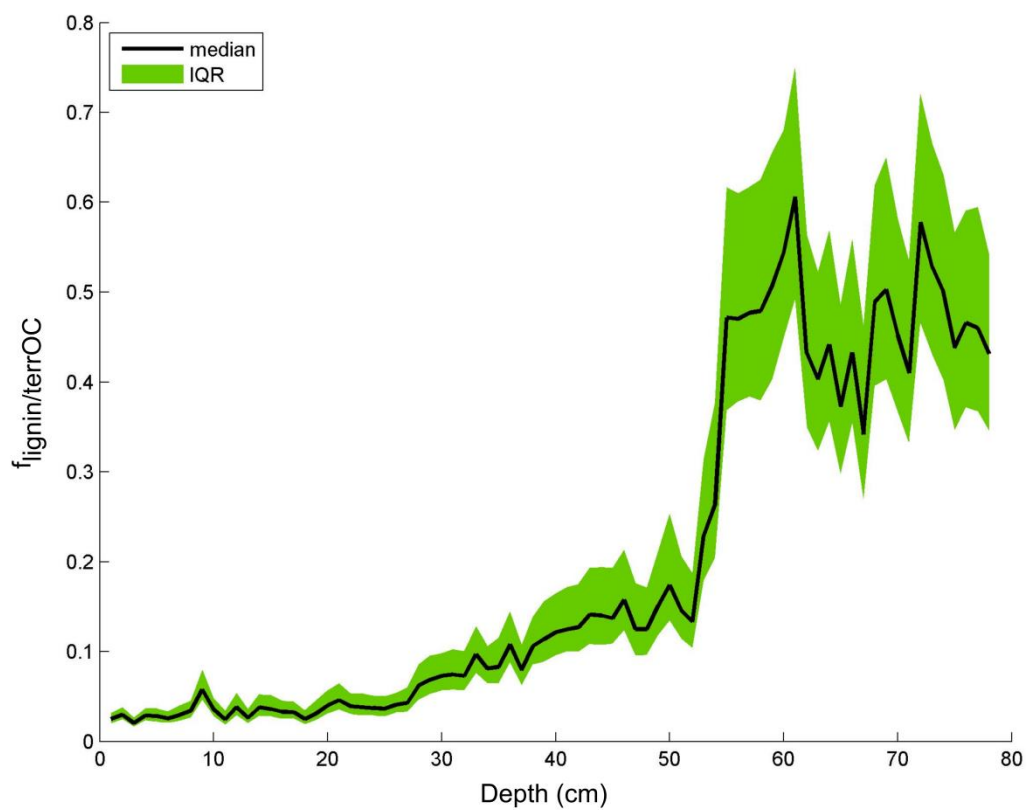
36 **Figure S3. Degradation proxies for terrestrial organic carbon in the sediment core GC58. The x-axis has**
 37 **breaks due to gaps in the sediment chronology. (a) Syringyl acid to syringaldehyde (Sd/SI) and vanillic acid to**
 38 **vanillin (Vd/Vl) ratios are a lignin-phenol based degradation proxy. The variability at the core top may also**
 39 **reflect the analytical uncertainty caused by very low lignin concentrations. (b) Also the ratio of 3,5-**
 40 **dihydrobenzoic acid to vanillyl phenols (3,5-Bd/V) provides information on degradation of terrestrial organic**
 41 **carbon. Higher values imply more degraded material for all the ratios as illustrated with the blue triangle.**
 42 **The 3,5-Bd/V values suggest a gradual increase in degradation from the bottom of the core to the top.**

43

44



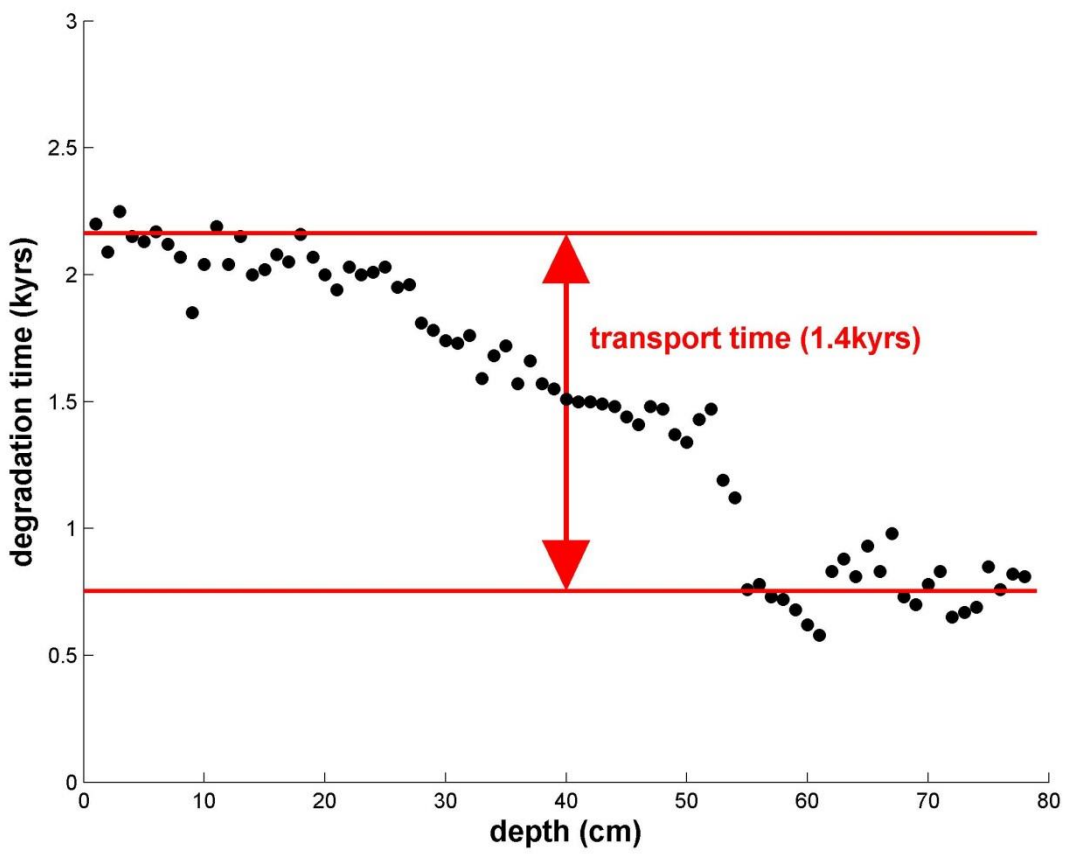
45

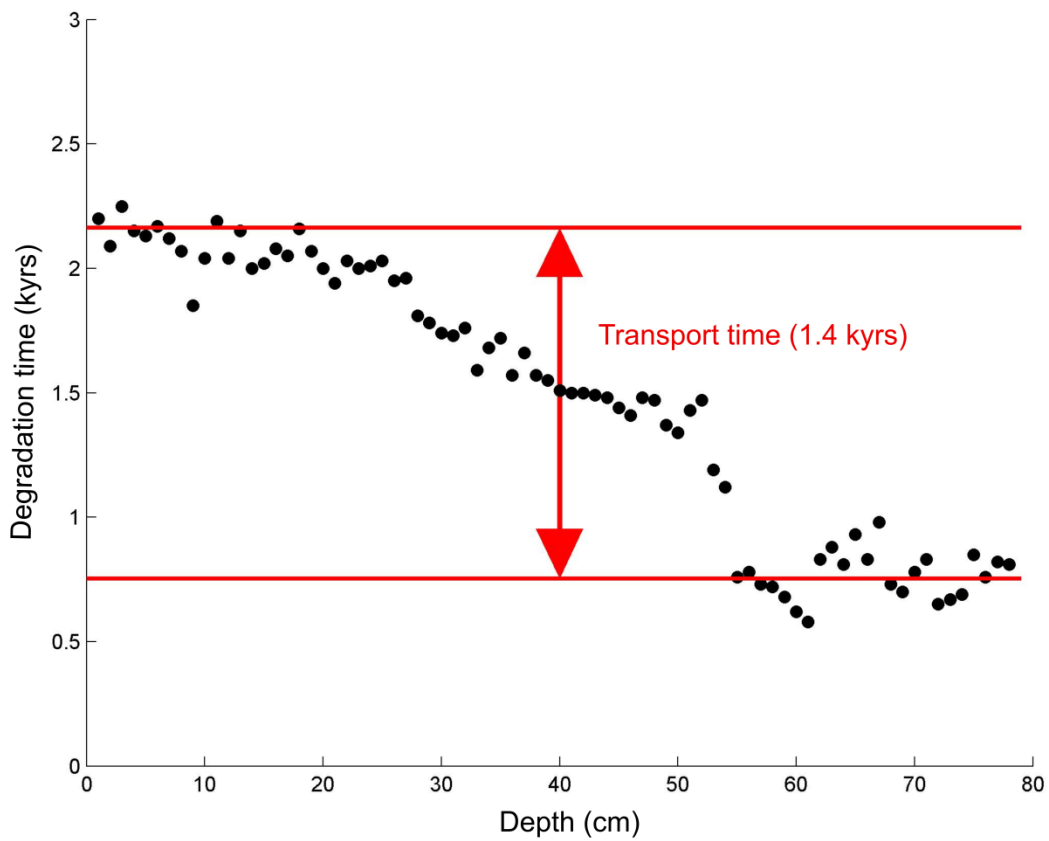


46

47 **Figure S34.** The ratio between the observed and expected lignin and terrestrial organic carbon (terrOC)
48 ratios ($f_{\text{lig/terrOC}}$) with interquartile range (IQR) for the sediment core GC58. The expected lignin values i.e.
49 non-degraded lignin are taken from Tesi et al., (2016). See Supplementary Methods for details.

50





52

53 **Figure S45.** An ~~estimate~~ ~~estimation~~ of the lateral transport time of sediments shown as the degradation time
54 (kyr) against the core depth (cm) in the sediment core GC58. See Supplementary Methods for lateral
55 transport time calculations.

56 Supplementary methods

57 Source apportionment calculations

58 In the model for smoothly varying source proportions, data is split into three time-segments of contiguous
59 observations. For each segment, observed $\delta^{13}C$ and $\Delta^{14}C$ are modelled as

60

$$\begin{aligned}\delta^{13}C_i &= \delta^{13}C^{ICD-PF} \times p_i^{ICD-PF} + \delta^{13}C^{TS-PF} \times p_i^{TS-PF} + \delta^{13}C^{M OC} \times p_i^{M OC} + \epsilon_i^{13}, \\ \Delta^{14}C_i &= \Delta^{14}C^{ICD-PF} \times p_i^{ICD-PF} + \Delta^{14}C^{TS-PF} \times p_i^{TS-PF} + \Delta^{14}C^{M OC} \times p_i^{M OC} + \epsilon_i^{14},\end{aligned}$$

61

62 where ϵ_i^{13} and ϵ_i^{14} are independent zero-mean normally distributed residuals with variances σ_{i3}^2 and σ_{i4}^2
63 respectively. Residual variances are assumed equal for the three time-segments. ICD-PF refers to Ice Complex
64 Deposit permafrost, TS-PF to topsoil permafrost and M OC to marine organic carbon.

65 The end-member values $\delta^{13}C^{ICD-PF}$, $\delta^{13}C^{TS-PF}$, $\delta^{13}C^{M OC}$, $\delta^{14}C^{ICD-PF}$, $\delta^{14}C^{TS-PF}$ and $\delta^{14}C^{M OC}$ are
66 assumed random effects shared within each time-segment and independent between. With the exception of
67 $\delta^{14}C^{ICD-PF}$ they are assumed normally distributed, with means and standard deviations reported earlier. To avoid
68 values below -1000, $\delta^{14}C^{ICD-PF} + 1000$ is instead assumed to be exponentially distributed. Due to different times
69 of deposit, $\delta^{14}C^{ICD-PF}$ means are set to -933, -833 and -800 for the younger, middle and older segment
70 respectively.

71 In order to account for the time-dependence between proportions, we follow an approach related to that of
72 Parnell et al. (20123) by modelling p_i^{ICD-PF} , p_i^{TS-PF} and $p_i^{M OC}$ using Bayesian cubic B-splines after a
73 transformation to the real plane using the additive log-ratio transform,

74

$$\begin{aligned}p_i^{ICD-PF} &= \frac{\exp(s_1(y_i))}{\exp(s_1(y_i)) + \exp(s_2(y_i)) + 1}, \\ p_i^{TS-PF} &= \frac{\exp(s_2(y_i))}{\exp(s_1(y_i)) + \exp(s_2(y_i)) + 1},\end{aligned}$$

75

76 and $p_i^{M OC} = 1 - p_i^{ICD-PF} - p_i^{TS-PF}$. The functions s_1 and s_2 are the spline-functions and y_i estimated years BP for
77 observation i . Separate/independent splines are used for each of the three time-segments and knots are placed at the
78 centres and endpoints. The model is fitted using rjags (Plummer, 2016) within the R computing environment (R
79 Core Team, 2016). The code for the model is available at https://github.com/mskoldSU/Keskitalo_et_al.

80 Lateral transport time estimation

81 The GC58 core spans over a time period of ~ 9,500 cal yrs BP, during which the study area experienced a
82 significant sea level rise (34 m in water depth). This means that the time for lateral transport of the terrestrial
83 organic carbon (terrOC) from the shore to the site of sedimentation increased. To model this transport time the ratio
84 of lignin/terrOC was used as a molecular clock. The fraction remaining lignin/terrOC ($f_{lig/terrOC}$) from
85 remineralisation depends on the degradation of both lignin and terrOC. Bröder et al. (2017, submitted) established
86 the following relation for the Laptev Sea (time t in kyrs):

87

$$88 \quad f_{lig/terrOC}(t) = \frac{e^{-2.6 \cdot t}}{0.87 \cdot e^{-2.2 \cdot t} + 0.13} \quad (2)$$

89 The observational concentration terrOC can be established as $OC/(1 - f_{\text{marine}})$, where the fraction marine is derived
90 from the source apportionment results. To obtain the observational $f_{\text{lig/terrOC}}$ we need to consider the expected
91 lignin/terrOC signal for the sources that have not been degraded. For ICD-PF the lignin/terrOC ratio is $17.4 \pm 8.3 \text{ mg}$
92 g^{-1} and for topsoil-PF $20.9 \pm 6.4 \text{ mg g}^{-1}$ (Tesi et al., 2016). Since the relative proportions of ICD-PF and topsoil-PF
93 for each data point is known from the source apportionment, the non-degraded lignin/terrOC signatures may be
94 estimated, using MCMC techniques to account for the end-member variability. By computing the ratio of the
95 observed and non-degraded lignin/terrOC ratios we can calculate the fraction remaining lignin/terrOC and further,
96 estimate the lateral transport times using Eq. (2).

97

98 **References**

- 99 Bröder, L., Tesi, T., Andersson, A., Semiletov, I. and Gustafsson, Ö.: Bounding cross-shelf transport time and
100 degradation in land-ocean carbon transfer. 2017. (submitted)
- 101 Parnell, A. C., Phillips, D. L., Bearhop, S., Semmens, B. X., Ward, E. J., Moore, J. W., Jackson, A. L. [Kelly, D. J](#)
102 and Inger, R.: Bayesian Stable Isotope Mixing Models, [arXiv Prepr. arXiv ..., 16](#), [Environmetrics, 24\(6\), 387–399](#),
103 doi:10.1002/env.2221, 2013.
- 104 Plummer, M.: rjags: Bayesian Graphical Models using MCMC., 2016.
- 105 R Core Team: R: A language and environment for statistical computing, 2016.
- 106 Tesi, T., Semiletov, I., Hugelius, G., Dudarev, O., Kuhry, P. and Gustafsson, Ö.: Composition and fate of
107 terrigenous organic matter along the Arctic land-ocean continuum in East Siberia: Insights from biomarkers and
108 carbon isotopes, *Geochim. Cosmochim. Acta*, 133, 235–256, doi:10.1016/j.gca.2014.02.045, 2014.
- 109 Tesi, T., Muschitiello, F., Smittenberg, R. H., Jakobsson, M., Vonk, J. E., Hill, P., Andersson, A., Kirchner, N.,
110 Noormets, R., Dudarev, O., Semiletov, I. and Gustafsson, Ö.: Massive remobilization of permafrost carbon during
111 post-glacial warming, *Nat. Commun.*, 7, 13653, doi:10.1038/ncomms13653, 2016.

112